The Type I / Type II Cytochrome c3 Complex: an Electron Transfer Link in the Hydrogen-Sulfate Reduction Pathway

ARTICLE *in* JOURNAL OF MOLECULAR BIOLOGY · DECEMBER 2005

Impact Factor: 4.33 · DOI: 10.1016/j.jmb.2005.09.036 · Source: PubMed

9 AUTHORS, INCLUDING:

Xavier Morelli
French National Centre for Scientific Resea…
54 PUBLICATIONS **998** CITATIONS
SEE PROFILE

Elisabeth Lojou
French National Centre for Scientific Resea…
88 PUBLICATIONS **1,355** CITATIONS
SEE PROFILE

Pascale Barbier
Aix-Marseille Université
48 PUBLICATIONS **1,015** CITATIONS
SEE PROFILE

Françoise Guerlesquin
Institute of Microbiology of the Mediterrane…
121 PUBLICATIONS **2,586** CITATIONS
SEE PROFILE

doi:10.1016/j.jmb.2005.09.036 J. Mol. Biol. (2005) 354, 73–90

JMB

Available online at www.sciencedirect.com

SCIENCE DIRECT®

ELSEVIER

The Type I / Type II Cytochrome c_3 Complex: an Electron Transfer Link in the Hydrogen-Sulfate Reduction Pathway

Laetitia Pieulle[1], Xavier Morelli[1], Philippe Gallice[2], Elisabeth Lojou[1] Pascale Barbier[3], Mirjam Czjzek[4], Pierre Bianco[1] Françoise Guerlesquin[1] and E. Claude Hatchikian[1]*

[1]*Unité de Bioénergétique et Ingéniérie des Protéines, Institut de Biologie Structurale et Microbiologie, CNRS, 31 chemin Joseph-Aiguier, 13402 Marseille Cedex 20, France*

[2]*Laboratoire de Chimie Générale et Prevention des Risques et Nuisances Technologiques Faculté de Pharmacie, 27 bd. Jean Moulin, 13385 Marseille Cedex 05, France*

[3]*ISPDCT, FRE-CNRS 2737 Faculté de Pharmacie, 27 bd. Jean Moulin, 13385 Marseille Cedex 05, France*

[4]*Architecture et Fonction des Macromolécules Biologiques Institut de Biologie Structurale et Microbiologie, CNRS, 31 chemin Joseph-Aiguier, 13402 Marseille Cedex 20, France*

**Corresponding author*

In *Desulfovibrio* metabolism, periplasmic hydrogen oxidation is coupled to cytoplasmic sulfate reduction *via* transmembrane electron transfer complexes. Type II tetraheme cytochrome c_3 (TpII-c_3), nine-heme cytochrome *c* (9HcA) and 16-heme cytochrome *c* (HmcA) are periplasmic proteins associated to these membrane-bound redox complexes and exhibit analogous physiological function. Type I tetraheme cytochrome c_3 (TpI-c_3) is thought to act as a mediator for electron transfer from hydrogenase to these multihemic cytochromes. In the present work we have investigated *Desulfovibrio africanus* (*Da*) and *Desulfovibrio vulgaris* Hildenborough (*Dv*H) TpI-c_3/TpII-c_3 complexes. Comparative kinetic experiments of *Da* TpI-c_3 and TpII-c_3 using electrochemistry confirm that TpI-c_3 is much more efficient than TpII-c_3 as an electron acceptor from hydrogenase (second order rate constant $k=9\times10^8$ M^{-1} s^{-1}, $K_m=0.5$ μM as compared to $k=1.7\times10^7$ M^{-1} s^{-1}, $K_m=40$ μM, for TpI-c_3 and TpII-c_3, respectively). The *Da* TpI-c_3/TpII-c_3 complex was characterized at low ionic strength by gel filtration, analytical ultracentrifugation and cross-linking experiments. The thermodynamic parameters were determined by isothermal calorimetry titrations. The formation of the complex is mainly driven by a positive entropy change ($\Delta S=137(\pm7)$ J mol^{-1} K^{-1} and $\Delta H=5.1(\pm1.3)$ kJ mol^{-1}) and the value for the association constant is found to be $(2.2(\pm0.5))\times10^6$ M^{-1} at pH 5.5. Our thermodynamic results reveal that the net increase in enthalpy and entropy is dominantly produced by proton release in combination with water molecule exclusion. Electrostatic forces play an important role in stabilizing the complex between the two proteins, since no complex formation is detected at high ionic strength. The crystal structure of *Da* TpI-c_3 has been solved at 1.5 Å resolution and structural models of the complex have been obtained by NMR and docking experiments. Similar experiments have been carried out on the *Dv*H TpI-c_3/TpII-c_3 complex. In both complexes, heme IV of TpI-c_3 faces heme I of TpII-c_3 involving basic residues of TpI-c_3 and acidic residues of TpII-c_3. A secondary interacting site has been observed in the two complexes, involving heme II of *Da* TpII-c_3 and heme III of *Dv*H TpI-c_3 giving rise to a TpI-c_3/TpII-c_3 molar ratio of 2:1 and 1:2 for *Da* and *Dv*H complexes, respectively. The physiological significance of these alternative sites in multiheme cytochromes *c* is discussed.

Keywords: type I cytochrome c_3; type II cytochrome c_3; protein interaction; microcalorimetry; nuclear magnetic resonance

Present address: M. Czjzek, Station Biologique de Roscoff, Végétaux Marins et Biomolécules UMR 7139, Place Georges Teissier, BP 74, 29682 Roscoff Cedex, France.

Abbreviations used: TpI-c_3, type I cytochrome c_3; TpII-c_3, type II cytochrome c_3; 9HcA, nine-heme cytochrome *c*; HmcA, 16-heme cytochrome *c*; *Da*, *Desulfovibrio africanus*; *Dv*H, *Desulfovibrio vulgaris* Hildenborough; *Dv*E, *Desulfovibrio vulgaris* Essex; SRB, sulfate-reducing bacteria; CV, cyclic voltammetry; ITC, isothermal titration calorimetry.

E-mail address of the corresponding author: hatch@ibsm.cnrs-mrs.fr

Introduction

Sulfate-reducing bacteria (SRB) are a group of anaerobes, which derive energy from the dissimilatory reduction of sulfate, using hydrogen or organic substrates as electron donors.[1] A great number of electron carriers exhibiting low redox potentials have been characterized in these bacteria;[2] however, the sulfate respiratory process is still poorly understood. In particular, the terminal reductases involved in sulfate reduction are cytoplasmic and therefore do not contribute directly to the production of a proton gradient across the membrane. Hydrogen metabolism plays a central role in energy-generating mechanisms of these microorganisms.[3] *Desulfovibrio* species can either consume H_2 through a transmembrane redox process linked to sulfate reduction[4,5] or produce hydrogen when growing fermentatively on pyruvate or lactate.[6–8] Hydrogenase is the key enzyme of hydrogen metabolism and has been found to be mostly confined to the periplasmic space.[9,10]

The SRB belonging to the genus *Desulfovibrio* have been studied extensively and are characterized by having an unusually high number of periplasmic multiheme cytochromes *c* with low-redox potential. These cytochromes appear to be involved in the electron transfer linked to hydrogen oxidation.[11,12] The well-characterized type I cytochrome c_3 (M_r 13,000) (TpI-c_3)[13] is the most abundant and is present in all *Desulfovibrio* species. It plays an important role in the metabolism acting as a physiological partner of hydrogenase.[14–16] Despite the low sequence homology between TpI-c_3 of different species, their three-dimensional structure shows a common topology organized around a four-heme cluster.[17–24] This four-heme structural motif appears to be a common feature for other members of the multiheme cytochromes *c*; examples include cytochrome c_3 (M_r 26,000), a dimer of the tetraheme unit[25,26] the 16-heme high molecular mass cytochrome *c* (HmcA),[27,28] the nine-heme cytochrome *c* (9HcA)[29,30] and the tetraheme type II cytochrome c_3 (TpII-c_3) which differs from TpI-c_3 by its biological and structural properties.[31–35]

The 16-heme Hmc, the nine-heme cytochrome and the four-heme TpII-c_3 display common genetic, functional and structural features. In genetic terms, these three multiheme cytochromes are encoded by a gene that is part of an operon encoding a membrane-bound redox complex,[34,36,37] whereas the genes for TpI-c_3[38] and cytochrome c_3 (26,000 M_r)[39] are monocistronic. The high degree of sequence homology between the subunits of the three transmembrane redox complexes suggests a functional similarity.[28] The three cytochromes display affinity for the membrane and share a common electron donor, the TpI-c_3, which acts as a mediator for electron transfer from periplasmic hydrogenases.[29,32,34,40,41] In contrast, the *Desulfovibrio desulfuricans* Essex (*Dd*E) nine-heme cytochrome *c* is a competent physiological electron acceptor for hydrogenase.[42] These observations support a key role of these multiheme cytochromes *c* in electron transfer from the periplasmic oxidation of hydrogen to the cytoplasmic reduction of sulfate. In the case of HmcA, this role is corroborated by growth and expression studies with wild-type and mutant strains of *Desulfovibrio vulgaris* Hildenborough (*Dv*H).[43–45] The structure of the three multiheme cytochromes *c* displays homologous domains. Indeed, the recent determination of the structure of HmcA from *Dv*H revealed that the protein comprises two TpII-c_3 domains and one 9HcA domain[27,28] whereas the nine-heme cytochrome was previously reported to be composed of two cytochrome c_3 1- like domains linked by a central bridging heme.[29,30] Moreover, surface charge mapping of *Dv*H TpII-c_3 and *Desulfovibrio desulfuricans* ATCC 27774 (*Dd*A27k) 9HcA indicates that they share similar characteristics that distinguish them from the TpI-c_3.[28] Indeed, TpII-c_3 can be distinguished from the TpI-c_3 overall fold by several local differences including the variety of loops with the most relevant point relative to surface electrostatic charges. TpII-c_3 is characterized by an exposed heme I surrounded by a negative surface charge whereas its heme IV lacks the typical surface lysine patch proposed to be the site of interaction and electron exchange of TpI-c_3 with a negatively charged region of hydrogenase.[33] This suggests that TpII-c_3 interacts with TpI-c_3 *via* heme I rather than heme IV.

The objective of this work was to characterize the complex formation between *Desulfovibrio africanus (Da)* TpI-c_3 and TpII-c_3 using various experimental techniques including kinetic analysis, analytical ultracentrifugation, microcalorimetry, NMR measurements and cross-linking experiments. These two redox partners constitute the most simple interprotein/redox complex involved in electron transfer from periplasmic hydrogen oxidation to cytoplasmic sulfate reduction. Several points including the data of the crystal structure of TpII-c_3[33] and the high efficiency of TpI-c_3 on TpII-c_3 reduction by hydrogenase[32] make the interaction between TpI-c_3 and TpII-c_3 from *Da* particularly appropriate to study. Although the three-dimensional structure of *Da* TpI-c_3 had not yet been determined, it was predicted that several conserved lysine residues in the C-terminal sequence of the protein may constitute a potential docking site for the hydrogenase redox partner.[32] We report also modelling studies of the TpI-c_3/TpII-c_3 complex in order to determine the structural properties of the complex interface. For this purpose, the crystal structure of *Da* TpI-c_3 has been solved at 1.5 Å resolution. Moreover, a structural model of the complex between *Dv*H TpI-c_3 and TpII-c_3 has been obtained by NMR restrained docking and allows a structural comparison with the *Da* TpI-c_3/TpII-c_3 complex.

Results

The *D. africanus* TpI-c_3/TpII-c_3 electron transfer complex

Kinetic studies of intermolecular electron transfer between D. africanus *hydrogenase and cytochromes* c$_3$

A periplasmic hydrogenase of the [NiFeSe]-type was previously identified in *Da*.[46] Kinetic data for the reaction between TpI-c_3 and hydrogenase under hydrogen atmosphere have been obtained from cyclic voltammetry (CV) curves. In the absence of enzyme, TpI-c_3 gave voltammograms consistent with a reversible electron exchange as already observed in previous work.[31] Upon addition of hydrogenase, the CV curve became sigmoidal with a pronounced catalytic anodic current (data not shown). Such an effect results from the continuous reduction of cytochrome by hydrogenase as described by the following sequence:

$$1/2\ H_2 + Hase_{ox} \rightarrow H^+ + Hase_{red}$$

$$Hase_{red} + cyt\ c_{3ox} \xrightarrow{k} Hase_{ox} + cyt\ c_{3red}$$

$$cyt\ c_{3red} \leftrightarrow cyt c_{3ox} + 4e^-$$

Analysis of the CV curves yielded a second-order rate constant k value of $9\times10^8\ M^{-1}\ s^{-1}$. The variation of the pH of the buffer solution showed that the highest catalytic current was obtained for a pH value of 8.5. The Michaelis constant K_m was estimated to be 0.5 μM at pH 8.5 for TpI-c_3 from the CV curves.

TpII-c_3 was unable to transfer electrons directly from or to the electrode in conditions of low ionic strength. It can be assumed that the high degree of negative charges on the surface of the protein prohibits the electron transfer to a negative charged electric interface.[47] In contrast, the addition of small amounts of TpI-c_3 yielded the electrochemical promotion of TpII-c_3, as denoted by the increasing CV peak currents obtained for TpII-c_3 in the presence of TpI-c_3 (Figure 1(a)). Promoted electron transfer for TpII-c_3 at a graphite electrode was already observed using poly-L-lysine,[47] thus suggesting that promotion could result from an ionic strength effect. This point has been confirmed in this work by experiments that were performed in the presence of 200 mM Tris–HCl. These results are indicative of the need of a positive electrochemical interface (which reduces electrostatic repulsion) for the electron transfer on TpII-c_3 to be achieved. The electrochemical behavior of TpII-c_3 has two main consequences. On one hand, no catalytic process can be observed when TpII-c_3 and hydrogenase are

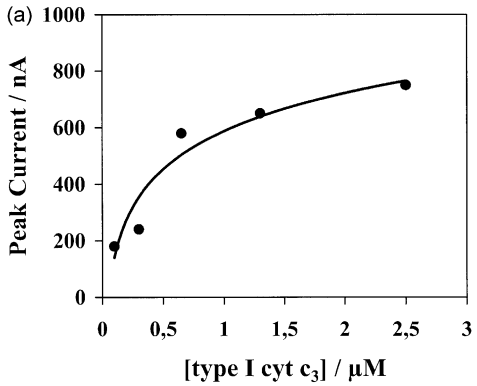

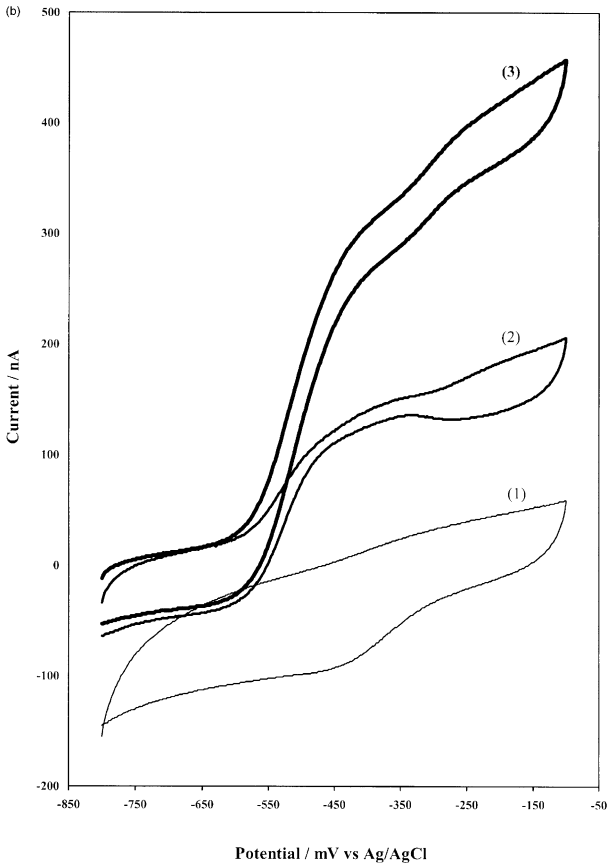

Figure 1. (a) Electrochemical promotion of TpII-c_3 by TpI-c_3. Scan rate, 20 mV s^{-1}, 50 mM Tris–HCl buffer (pH 8.5). (b) Electrocatalytic oxidation of hydrogen *via D. africanus* hydrogenase and TpII-c_3 promoted by TpI-c_3. (1) CV curve for 0.6 μM TpI-c_3 and 27 μM TpII-c_3. (2) CV curve for 0.6 μM TpI-c_3 in the presence of 115 nM hydrogenase. (3) CV curve for 0.6 μM TpI-c_3 and 27 μM TpII-c_3 in the presence of 115 nM hydrogenase. Scan rate, 5 mV s^{-1}, 50 mM Tris–HCl buffer (pH 8.5).

reacting under low ionic strength conditions. On the other hand, electrocatalytic current developed when adding TpI-c_3 aliquots to TpII-c_3, or when TpII-c_3 and hydrogenase are reacting under higher ionic strength conditions (i.e. 200 mM Tris–HCl). Figure 1(b) shows the characteristic anodic current relative to the reaction between TpII-c_3 and hydrogenase promoted by TpI-c_3. The analysis of the electrochemical response yielded a second-order rate constant for the reaction between promoted TpII-c_3 and hydrogenase of $1.7\times10^7\ M^{-1}\ s^{-1}$ at pH 8.5. Under these conditions, a K_m value for TpII-c_3 of about 40 μM at pH 8.5 was determined from CV curves. It is interesting to note that a similar value of $1.6\times10^7\ M^{-1}\ s^{-1}$ is calculated from CV curves recorded for the catalytic reaction between TpII-c_3 and hydrogenase in 200 mM Tris–HCl. Thus, the kinetic data obtained from electrochemical measurements clearly underline that TpI-c_3 is at least 50 times more efficient than TpII-c_3 in the hydrogen consumption reaction *via* hydrogenase.

Evidence for complex formation between *Da* TpI-c_3 and TpII-c_3

Molecular exclusion chromatography

Previous studies showed that *Da* TpII-c_3 can interact with hydrogenase, but the electron transfer process is greatly improved in the presence of TpI-c_3.[32] Additional evidence for complex formation between the two redox partners can be deduced from gel filtration experiments (data not shown). When subjected to size exclusion chromatography on Sephadex G-75 at low ionic strength, TpI-c_3 and TpII-c_3 migrate with an apparent M_r value of 15,500 Da and 21,000 Da, respectively. Under these conditions, a good correlation was observed between the known molecular mass of TpI-c_3 (15,102 Da)[32] and the molecular mass calculated from its elution volume, whereas the value estimated in this way for TpII-c_3 was clearly higher as compared to its known molecular mass (13,742 Da).[32] This anomalous behaviour, which may be due to the strong acidic properties of TpII-c3,[48] disappeared when gel filtration was performed at moderate ionic strength. When the two cytochromes c_3 are subjected together to gel filtration on Sephadex G-75 at low ionic strength, TpI-c_3 co-migrates with TpII-c_3 with an apparent M_r value for the complex of 32,000 Da. If the chromatography on Sephadex G-75 was repeated under conditions where the electrostatic complex would be expected to dissociate (in buffer supplemented with 50 mM NaCl) no co-migration was observed and TpI-c_3 and TpII-c_3 eluted as single peaks with an apparent molecular mass of 15,000 Da close to their respective molecular masses. These observations are indicative of a complex formation between the two cytochromes c_3 and provide evidence for the importance of electrostatic forces in the stabilization of the complex. However, the stoichiometry of the complex could not be determined accurately from the gel filtration experiments due to the anomalous behaviour of TpII-c_3. Therefore, other methods including analytical ultracentrifugation, microcalorimetry and NMR spectroscopy have been used to measure this parameter.

Analytical ultracentrifugation

Analysis of a large concentration range of TpI-c_3 by a single sedimenting species model led to a weight-average molecular mass (M_w) of 15,373(±1066) Da, in good agreement with the theoretical mass of this cytochrome (15,102 Da).[32] In the same way, the single sedimenting species model analysis of TpII-c_3 gave an estimated molecular mass of 13,166(±2077) Da, in accordance with its theoretical mass (13,742 Da).[32] These results confirm those previously found[31] and indicate that both *Da* cytochromes c_3 behave as a monomer in solution.

The interaction between these two cytochromes was subsequently investigated by sedimentation equilibrium using various mixtures of both cytochromes containing a fixed concentration of TpII-c_3 (0.25 mg/ml) and increasing concentrations of TpI-c_3 (from 0.01 mg/ml to 2.8 mg/ml). The equilibrium concentration gradient was fitted by a model with a single sedimenting species. The apparent molecular masses (M_w) calculated by the way were divided by the apparent molecular mass of the TpII-c_3 alone to determine the apparent stoichiometry of the TpI-c_3/TpII-c_3 complex. A sigmoidal increase of the ratio from 1 to a value of about 3 was obtained when raising the concentration of TpI-c_3, suggesting a stoichiometry of 2:1 for the complex formed by TpI-c_3 and TpII-c_3, respectively (Figure 2).

Formation of TpI-c_3 and TpII-c_3 cross-linked complex

Covalent cross-linking experiments were performed to investigate the direct binding between TpI-c_3 and TpII-c_3. When TpI-c_3 and TpII-c_3 were treated with CME-CDI, the analysis of the reaction mixture by SDS-polyacrylamide gel electrophoresis showed the formation of cross-linked products. The major band observed corresponds to a covalent complex of relative molecular mass around 30 kDa (Figure 3, lane 4). This mass corresponds to that of a binary complex and the amino acid composition of the 30 kDa cross-linked species is in agreement with a stoichiometric molar ratio of 1:1 between the two cytochromes (data not shown). We detected also a minor cross-linked product of apparent mass around 43 kDa. This mass could correspond to covalent cross-linking between TpI-c_3 and TpII-c_3 with a stoichiometric molar ratio of 2:1 resulting in the formation of a ternary complex (Figure 3, lane 4). As a control, incubation of either TpI-c_3 or TpII-c_3 alone with CME-CDI induced no cross-linked products (Figure 3, lanes 1 and 2).

The production of covalent complexes through the use of carbodiimide suggests that the specific TpI-c_3/TpII-c_3 binding involves electrostatic interactions

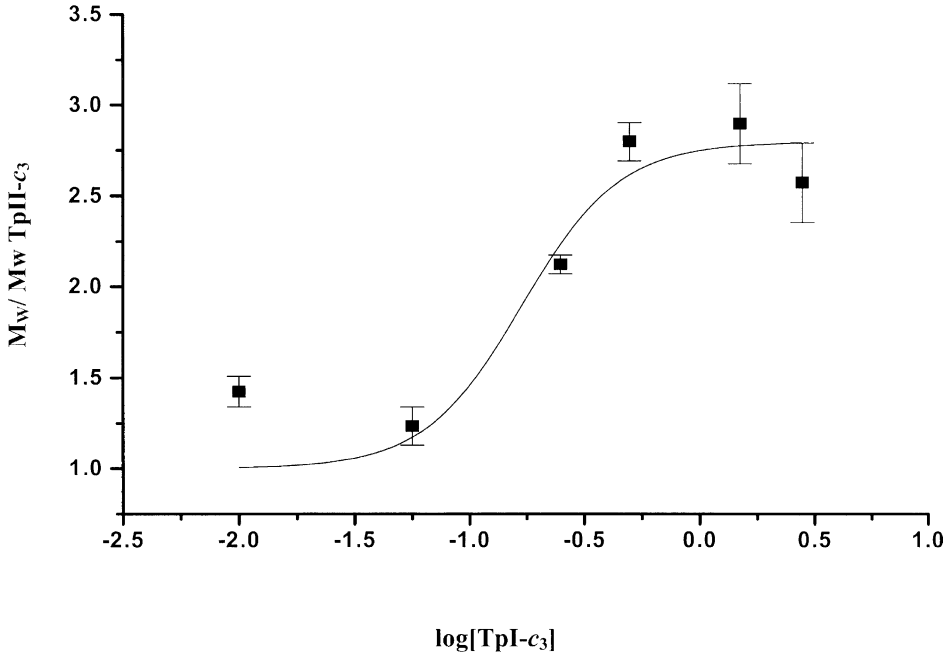

Figure 2. Sedimentation equilibrium analysis of the TpI-c_3/TpII-c_3 complex. Dependence of the ratio of the weight-average apparent molecular mass (M_w) of the TpI-c_3/TpII-c_3 complex *versus* the weight-average molecular mass of TpII-c_3 (0.25 mg/ml) as a function of the log of TpI-c_3 concentration (from 0.01 mg/ml to 2.8 mg/ml). Black squares represent experimental values. Error bars indicate the standard deviation. The continuous line shows the tendency of the curve.

between negatively charged residues and lysyl residues. Moreover, the increase of the ionic strength prevents the cross-linking reaction between TpI-c_3 and TpII-c_3. We observed a decrease of the cross-linked products with the increase of NaCl concentration in the range 0–400 mM (Figure 3, lanes 4–7). This result is in accordance with the establishment of ionic pairs during the complex formation.

Characterization of the TpI-c_3/TpII-c_3 complex by ITC

A typical set of data for the TpI-c_3/TpII-c_3 interaction in 10 mM cacodylate buffer (pH 5.5) is shown in Figure 4(a). The upper panel presents the raw calorimetric data for the titration and the lower panel the corresponding binding isotherm. From the titration curves issued from two independent experiments, the stoichiometry of the complex formation is calculated to be two molecules of *Da* TpI-c_3 per molecule of TpII-c_3. The association constant mean value is $K_a = (2.2(\pm 0.5)) \times 10^6\ M^{-1}$. The heat of binding is endothermic, the observed enthalpy change mean value is $\Delta H^0_{obs} = 16.4(\pm 1.3)$ kJ mol^{-1} of TpI-c_3, and the entropy change mean value is $\Delta S^0_{obs} = 174(\pm 6)$ J mol^{-1} K^{-1}. The ΔH^0_{obs} and ΔS^0_{obs} values are compatible with a hydrophobic interaction contributing to the complex formation.

Effect of ionic strength on binding

The dependence of the TpI-c_3/TpII-c_3 binding according to ionic strength was determined by adding NaCl to the buffer and keeping the pH constant. The association constant decreases from $K_a = 2.2 \times 10^6 (\pm 0.5 \times 10^6)\ M^{-1}$ at 0 mM NaCl to $K_a = 0.14 \times 10^6\ (\pm 0.01 \times 10^6)\ M^{-1}$ at 50 mM NaCl. The enthalpy changes at these ionic strengths are $\Delta H^0_{obs} = 16.4(\pm 1.3)$ kJ mol^{-1} and $\Delta H^0_{obs} = 13.2(\pm 1.1)$ kJ mol^{-1}, respectively. At 100 mM NaCl and 10 μM TpI-c_3 concentration, the K_a value is too weak to be determined. As increasing ionic strength induces a strong decrease of the association constant, our results clearly show that electrostatic interactions are involved in the binding of the two proteins.

Effect of pH on binding

The pH dependence of *Da* TpI-c_3/TpII-c_3 complex formation was studied at pH 5.5 in

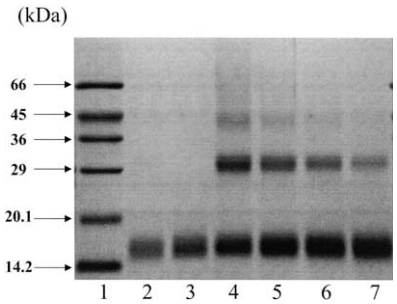

Figure 3. SDS-PAGE of *D. africanus* TpI-c_3-TpII-c_3 cross-linking. Cross-linking reactions between TpI-c_3 (75 μM) and TpII-c_3 (76 μM) were carried out in the presence of CME-CDI (15 mM) as described. Lane 1, molecular mass standard proteins; lane 2, TpII-c_3 treated with CME-CDI; lane 3, TpI-c_3 treated with CME-CDI; lane 4, TpI-c_3 and TpII-c_3 incubated with CME-CDI; lanes 5–7, as lane 4 at 100, 200 and 400 mM NaCl.

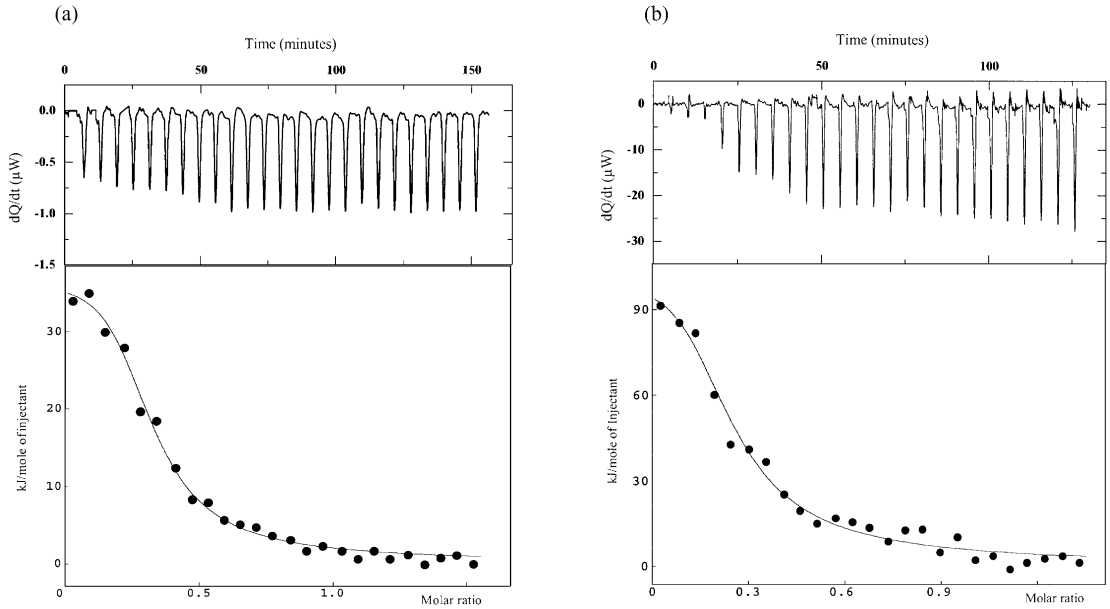

Figure 4. (a) Typical isothermal titration calorimetry of the binding of TpI-c_3 to TpII-c_3 from *D. africanus*. Upper panel: Raw data obtained for 25 injections, each of 3 μl, of TpII-c_3 solution (0.191 mM) into the sample cell containing TpI-c_3 solution (10.2 μM) in 10 mM cacodylate buffer (pH 5.5). Lower panel: Plot of processed data. The points are experimental and the continuous line corresponds to the best-fit curve. The best fitting parameters are 0.48 for stoichiometry, 2.8×10^6 M^{-1} for K_a, and 17.7 kJ/mol of TpI-c$_3$ for ΔH^0_{obs}. (b) Isothermal titration calorimetry of the binding of TpI-c_3 to TpII-c_3 from *D. vulgaris*. Upper panel: Raw data obtained for 25 injections, each of 3 μl, of TpI-c_3 solution (2.75 mM) into the sample cell containing TpII-c_3 solution (0.168 mM) in 2.5 mM phosphate buffer (pH 6.0). Lower panel: Plot of processed data. The points are experimental and the continuous line corresponds to the best-fit curve. The best fitting parameters are 0.47 for stoichiometry, 1.4×10^4 M^{-1} for K_a, and 44.2 kJ mol^{-1} of TpII-c_3 for ΔH^0_{obs}.

10 mM cacodylate or 5 mM Mes buffers, and at pH 6.0, pH 6.5 and pH 7.0 in 2.5 mM phosphate or 5 mM Mes buffers. Results show that the complex is more stable at pH 5.5 ($K_a = 2.2\times10^6(\pm0.5\times10^6)$ M^{-1}) and pH 6.0 ($K_a = 2.1\times10^6(\pm0.1\times10^6)$ M^{-1}) than at pH 6.5 ($K_a = 0.59\times10^6(\pm0.04\times10^6)$ M^{-1}). At pH 7.0 and 10 μM TpI-c_3 concentration the K_a value was too weak to be determined. Moreover, the enthalpy changes are endothermic in cacodylate ($\Delta H^0_{obs} = 16.4(\pm1.3)$ kJ mol^{-1}) and phosphate buffers ($\Delta H^0_{obs} = 10.0(\pm0.8)$ kJ mol^{-1} at pH 6.0, and $\Delta H^0_{obs} = 13.4(\pm1.1)$ kJ mol^{-1} at pH 6.5), whereas they are exothermic in Mes buffer ($\Delta H^0_{obs} = -25.7$, -13.3 and -11.9 kJ mol^{-1} at pH 5.5, pH 6.0 and pH 6.5, respectively). This reverse heat of binding observed while the K_a is analogous indicates that proton release occurred in the binding process. The observed enthalpy value (ΔH^0_{obs}) must be thus corrected to obtain the interaction enthalpy value (ΔH^0_{int}). As reported previously,[49] by calling N the change in the number of protons released upon binding of the ligand and so taken up by the buffer with a heat of neutralization (ΔH^b_n), the ΔH^0_{int} can be calculated according to the relation:

$$\Delta H^0_{int} = \Delta H^0_{obs} - N\Delta H^b_n$$

Taking into account the ΔH^b_n values that we determined for cacodylate, phosphate and Mes buffers used in our experiments, ($\Delta H_n^{cacodylate} = 5.4$ kJ mol^{-1}, $\Delta H_n^{phosphate} = -3.3$ kJ mol^{-1} and $\Delta H_n^{MES} = -14.6$ kJ mol^{-1}), N was calculated from the ΔH^0_{obs} measured in these buffers at constant pH value and found to be close to 2 mol of protons released per mol of TpI-c_3; the corresponding ΔH^0_{int} are reported in Table 1. As reported, the weak enthalpy changes, ΔH^0_{int}, and the large positive entropy values, ΔS^0_{int}, reflect an entropy-driven effect. Since, as mentioned above, the marked ionic strength effect clearly indicates an electrostatic contribution to the interaction, it is possible that the large positive entropy changes arise from exclusion of water molecules from the sites of interaction. Thus, the negative entropy change due to electrostatic interaction can be largely compensated by the positive entropy ΔS^0_{int} due to

Table 1. Effect of pH on *Da* TpI-c$_3$/TpII-c$_3$ binding

pH	$K_a\times10^6$ (M^{-1})	ΔG^0 (kJ mol^{-1})	ΔH^0_{obs} (kJ mol^{-1})	N	ΔH^0_{int} (kJ mol^{-1})	ΔS^0_{int} (J mol^{-1}K^{-1})
5.5	2.2 ± 0.5	-37.6 ± 0.6	16.4 ± 1.3	2.1	5.1 ± 1.3	137 ± 7
6.0	2.1 ± 0.1	-37.5 ± 0.1	10.0 ± 0.8	2.1	16.7 ± 0.8	175 ± 2
6.5	0.59 ± 0.04	-34.2 ± 0.2	13.4 ± 1.1	2.2	20.3 ± 1.1	176 ± 4

Thermodynamic parameter values are the mean$\pm$SD of two independent experiments conducted with TpI-c_3 and TpII-c_3 from *D. africanus*, for pH 5.5 in cacodylate, and for pH 6.0 and 6.5 in phosphate buffers, as described in the text.

the loss of water molecules. Proton release associated with water molecule exclusion dominates to result in a net increase in enthalpy and entropy. Moreover, the increase in ΔH^0_{int} and ΔS^0_{int} concomitant with a decrease of K_a as a function of pH seems to indicate that the ionization states of the proteins play a role in the TpI-c_3/TpII-c_3 complex formation.

Characterization at the molecular level of the interaction between *Da* TpI-c_3 and TpII-c_3

NMR titration of TpI-c_3/TpII-c_3 complex formation

The 1D-NMR titration of *Da* TpII-c_3 and TpI-c_3 complex formation is presented in Figure 5. The increase in the linewidth and the chemical shift variations of the heme methyl resonances found in the region 35 ppm to 16 ppm of both cytochromes indicate that a complex is formed, with a fast exchange at the NMR time scale. The titration of the complex formation observed for the heme methyl resonance at 31.18 ppm of TpI-c_3 is in agreement with a stoichiometry of two molecules of TpI-c_3 for one molecule of TpII-c_3 (Figure 6(a)). In the 1D-NMR spectra of TpII-c_3, two effects were observed: the methyl resonance at 17.75 ppm assigned to heme I[35] is first affected (Figure 6(b)) and after saturation the resonance at 25.25 ppm, assigned to heme II, is affected by the complex formation (Figure 6(c)). The chemical shift variations of TpII-c_3 resonances indicate the presence of two binding sites with higher affinity for heme I and a rather lower affinity for heme II.

Molecular model of TpI-c$_3$/TpII-c$_3$ complex

The overall structure of the *D. africanus* type I tetraheme cytochrome c_3 has been determined at 1.5 Å. The final model of *Da* TpI-c_3 contains two copies of the molecule, both comprising all 114 residues of the primary sequence, four heme groups (heme numbering is according to the appearance of the cysteine residues, covalently linking the heme groups, in the primary sequence), one calcium ion each and a total of 289 water molecules. The principal secondary structure elements indicated by the program DSSP[50] are a short, two-stranded antiparallel β-sheet in the N-terminal region (residues Asp6–Asp10 and Lys22–Ser26), an α-helix from Phe77 to Lys101, interrupted, as is typical in this type of cytochromes, by a six-residue containing loop and a high number of turns (Figure 7).

Although the TpI-c_3 could not be solved by molecular replacement using other known structures of cytochromes c_3 as search models, it displays high structural similarity with all cytochromes c_3 and clearly belongs to the same family. The four-heme cluster, characteristic of this type of cytochromes, superposes with a root-mean-square deviation of 0.35 Å and 0.30 Å to those of TpII-c_3 from *D. africanus* and TpI-c_3 from *D. gigas*, respectively.

An important factor governing the redox properties of the different heme groups in this type of protein is the heme solvent exposure. In this structure the heme solvent exposures, calculated with TURBO-FRODO using a 1.4 Å probe radius, are 153 Å^2, 253 Å^2, 202 Å^2 and 78 Å^2 for hemes I, II, III and IV, respectively. Interestingly, the exposure of heme IV is particularly low in this cytochrome c_3

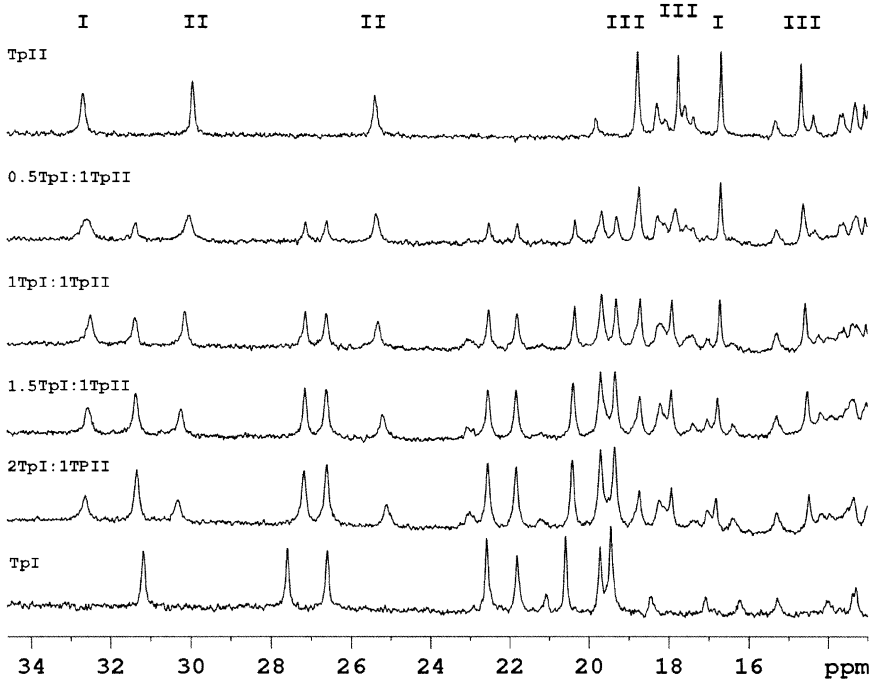

Figure 5. 1D-NMR titration of the *Da* TpI-c_3/TpII-c_3 complex formation. The 35–16 ppm region of the spectrum containing the heme methyl resonances is only shown. I, II and III indicate the heme assignment according to the structure numbering.[35] TpI and TpII refer to TpI-c_3 and TpII-c_3, respectively.

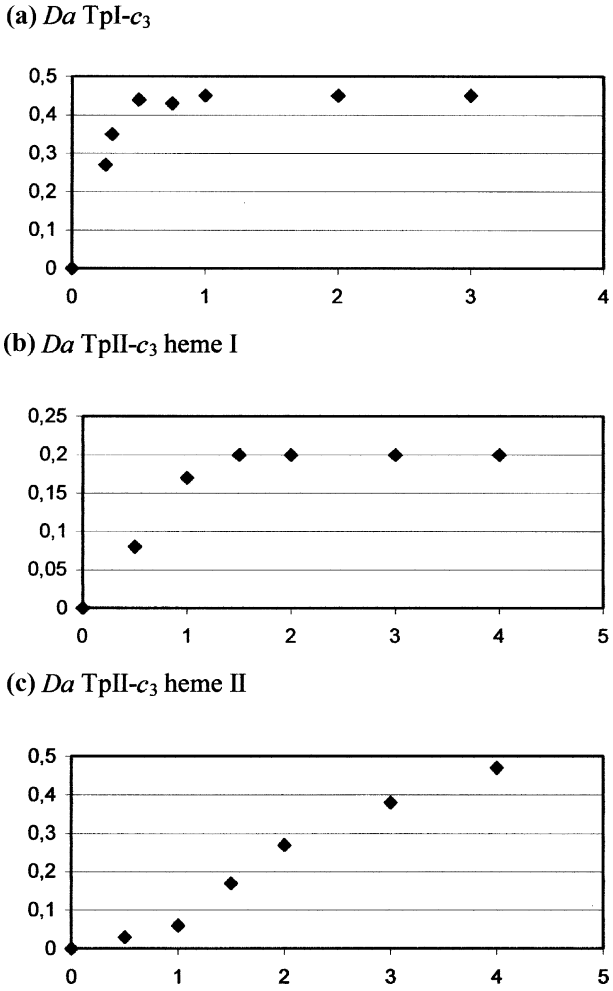

Figure 6. Titration curves of the *Da* TpI-c_3/TpII-c_3 complex formation from 1D-NMR data (Figure 5). (a) The chemical shift variations of the resonance at 31.18 ppm of TpI-c_3. (b) The chemical shift variations of the resonance at 17.75 ppm of heme methyl I of TpII-c_3. (c) The chemical shift variations of the resonance at 25.25 ppm of heme methyl II of TpII-c_3.

allowing its assignment to the high potential heme (−90 mV).[51] Another unusual feature of heme IV, although already observed once for TpI-c_3 from *D. gigas*,[22] is the presence of a calcium ion, tightly bound with octahedral coordination by the propionate groups of heme IV, the side-chains of Asp10 and Glu20 and the main-chain carboxyl groups of Leu12 and Tyr21.

Like in all basic TpI-c_3, 14 lysine residues are present in the primary sequence of *Da* cytochrome, ten of which are located in the loops surrounding heme IV (Figure 7). It has been shown by several methods[27,41,52–54] that this region around the solvent-exposed heme-edge of heme IV is the privileged zone of interaction of TpI-c_3 with their respective physiological partners.

An *ab initio* docking of the TpI-c_3/TpII-c_3 complex was calculated on the basis of the Protein Data Bank file 3cao for the TpII-c_3 and our PDB file for the TpI-c_3 (described here, PDB id code 2bq4), TpII-c_3 being

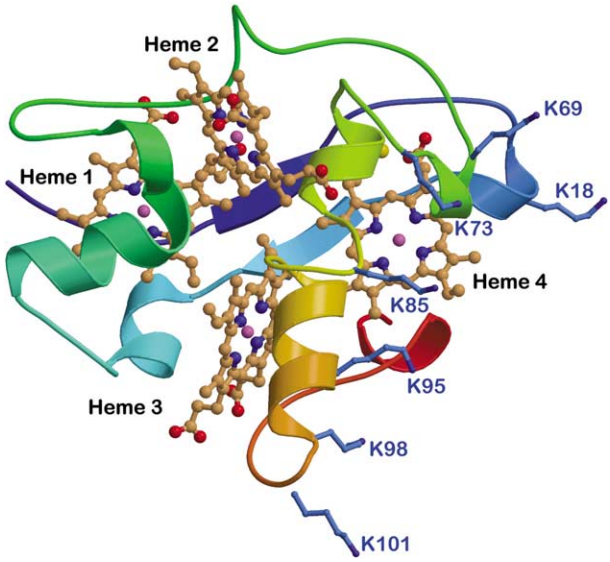

Figure 7. Ribbon representation of the type-I cytochrome c_3 from *D. africanus*. The ribbon is colored in the range from blue (N terminus) to red (C terminus). The four heme groups are numbered and the lysine residues surrounding heme 4 are highlighted. The Figure was prepared with MOLSCRIPT.

the target. One thousand putative structures of the complex were obtained from the software BiGGER. These structures were first evaluated and ranked by an *ab initio* procedure, which uses an interaction scoring function (Figure 8(a)). This representation clearly shows that two distinct sites are preferentially used for the docking, involving heme I and II of the TpII-c_3, while the heme IV of the TpI-c_3 is mostly involved in the interaction. The main interaction, based on the number of representatives of each family, is heme I for the TpII-c_3 and heme IV for the TpI-c_3. The electrostatic representations (Figure 8(a), second row) also pinpoint that only the heme IV environment of TpI-c_3 is positively charged and thus capable of an interaction with the isotropically negatively charged TpII-c_3. These purely theoretical calculations are in total agreement with the experimental results reporting a stoichiometry of two TpI-c_3 for one TpII-c_3 in this complex and the implication of heme I and II of TpII-c_3 during the NMR titration experiments, with a higher affinity for TpII-c_3 heme I.

The *D. vulgaris* Hildenborough TpI-c_3/TpII-c_3 electron transfer complex

Characterization of the complex by ITC

The set of data for the TpI-c_3/TpII-c_3 interaction is shown in Figure 4(b). The upper panel presents the raw calorimetric data for the titration and lower panel the corresponding binding isotherm. From the titration curve, the stoichiometry of the complex formation is calculated to be two molecules of TpII-c_3 per molecule of TpI-c_3. The association constant

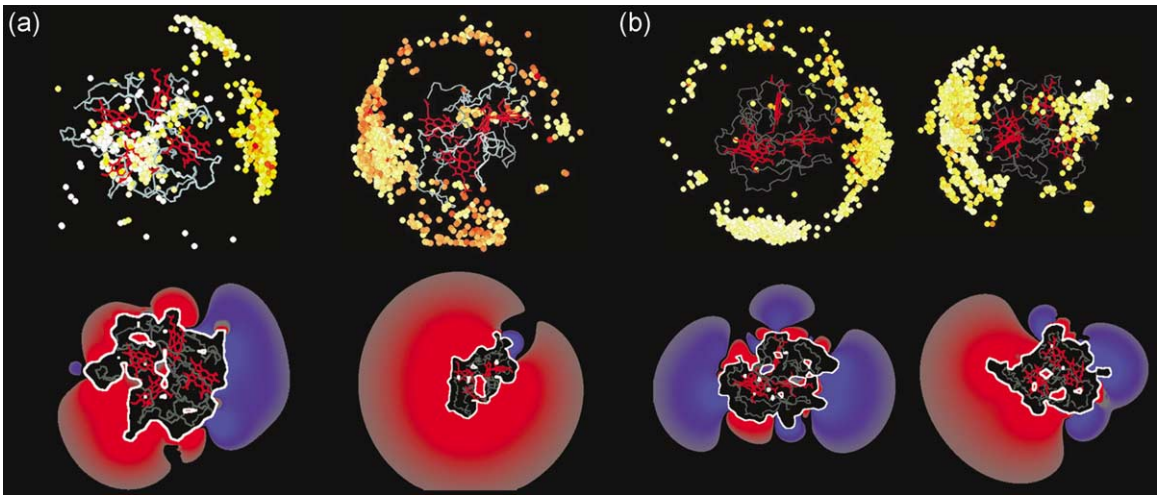

Figure 8. Docking of *Da* TpI-c_3/TpII-c_3 and *Dv*H TpI-c_3/TpII-c_3 complexes. The polypeptide chain of the cytochrome is colored in gray. Prosthetic groups of the cytochromes are colored red. Each ball represents the center of mass of the protein partner for one of the complexes. (a) *Da* TpI-c_3 and TpII-c_3 docking. Left, TpI-c_3 is the target protein and each sphere represents the center of mass of the position of one TpII-c_3. Right, TpII-c_3 is the target protein and each sphere represents the center of mass of the position of one TpI-c_3. The solutions are ranked with the BiGGER scoring function and represented by a colored scale from white (theoretically bad solutions) to red (theoretically good solutions). (b) Idem for *Dv*H TpI-c_3 and TpII-c_3 docking. The second row shows the electrostatic charge distribution for each cytochrome. The isopotential representation was performed with BiGGER, using the Poisson–Boltzmann equation. Basic charges are represented in blue and acidic residues in red. The cytochrome orientations are the same as in the first row.

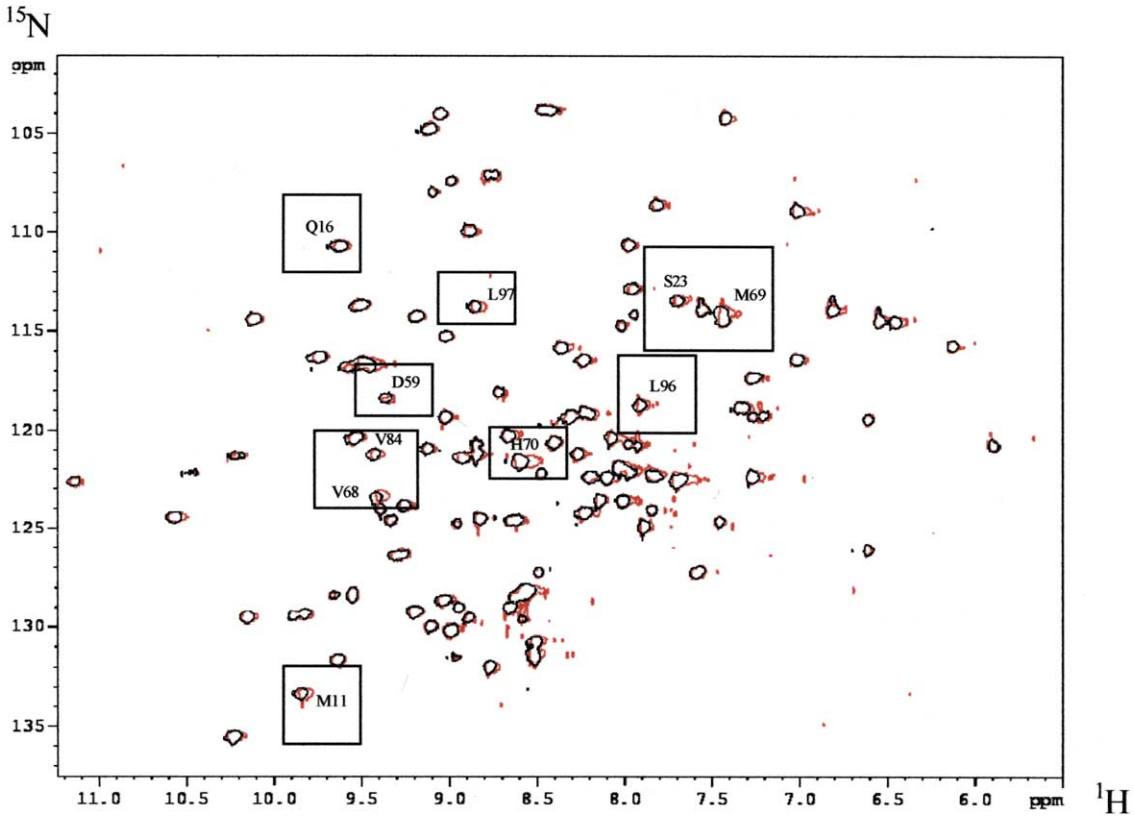

Figure 9. 2D-NMR mapping of TpII-c_3 interacting site on *Dv*H TpI-c_3. ^{1}H–^{15}N HSQC of TpI-c_3 was recorded in the absence (black) and presence (red) of TpII-c_3. The ten residues most affected by the interaction are indicated on the Figure (boxes and sequence numbering).

value is $K_a = 1.4 \times 10^4\ M^{-1}$. The heat of binding is endothermic, the observed enthalpy change value is $\Delta H^0_{obs} = 44.2\ kJ\ mol^{-1}$ of TpII-c_3, and the entropy change value is $\Delta S^0_{obs} = 222\ J\ mol^{-1}\ K^{-1}$.

Characterization at the molecular level of the complex

NMR titration of TpI-c3/TpII-c3 complex formation

Figure 9(a) presents a ^1H-^{15}N HSQC spectrum of *Dv*H TpI-c_3 already assigned.[55] The presence of TpII-c_3 induces important chemical shift variations of ten amide groups of the protein (M11, Q16, S23, D59, V68, M69, H70, V84, D96 and L97). These residues located at the interacting surface are distributed around heme III and heme IV.

Docking of TpI-c3/TpII-c3 complex

An *ab initio* docking of the complex was calculated on the basis of the Protein Data Bank file 2cth for the TpI-c_3 and our model for the TpII-c_3 (described here; see Materials and Methods), TpI-c_3 being the target. Here also, 1000 putative structures of the complex were obtained from the software BiGGER. These structures were first evaluated and ranked by an *ab initio* procedure, which uses the interaction scoring function (Figure 8(b)). An opposite result is observed here, compared to the docking of the *D. africanus* cytochromes. Two distinct sites are preferentially involved for the docking concerning heme III and IV of the TpI-c_3, while heme I of the TpII-c_3 is preferentially involved in the interaction. The main interaction site, regarding the number of representatives of each family, is here heme IV of TpI-c_3 and heme I of TpII-c_3. The electrostatic representations (Figure 8(b), second row) also pinpoint that only the environment of heme I of TpII-c_3 is negatively charged and thus capable of an interaction with the mainly positively charged heme of TpI-c_3. These purely theoretical calculations are again in total agreement with the experimental results reporting a stoichiometry of one TpI-c_3 for two TpII-c_3 in this complex and the implication of heme III and IV of TpI-c_3 during the NMR titration experiments. Here the heteronuclear NMR experiments permit us to apply the "restrained soft docking approach".[56] The amino acid residues from TpI-c_3 involved in the interaction with TpII-c_3, as seen by NMR, were used to filter out false positive solutions. The resulting

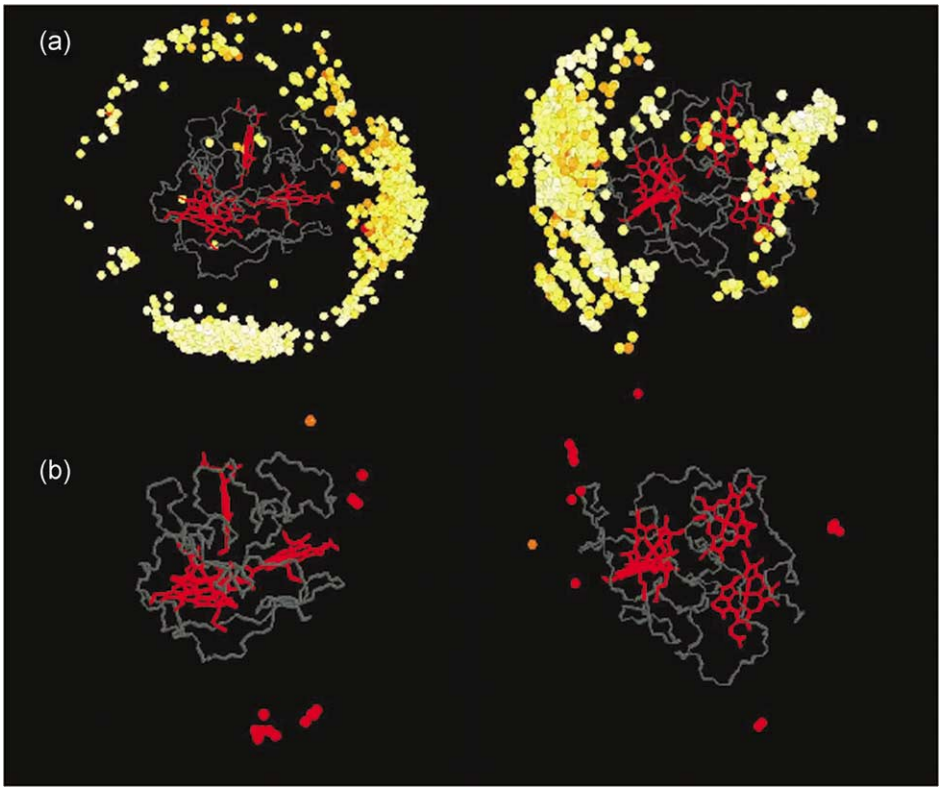

Figure 10. Restrained soft docking results of the TpI-c_3/TpII-c_3 complex from *Dv*H. The polypeptide chain of the cytochrome is colored gray. Prosthetic groups of the cytochromes are colored red. Left, TpI-c_3 is the target protein and each sphere represents the center of mass of the position of one TpII-c_3. Right, TpII-c_3 is the target protein and each sphere represents the center of mass of the position of one TpI-c_3. (a) The 1000 first *ab initio* docking solutions from BiGGER are shown. The solutions are ranked with the BiGGER scoring function and represented by a colored scale from white (bad solutions) to red (good solutions). (b) NMR filtering of the same solutions. The ten residues of the TpI-c_3 affected by the presence of TpII-c_3 were used to eliminate false positives from the *ab initio* models. The resulting solutions are represented as red spheres, showing two potential interacting sites on TpI-c_3 around hemes III and IV (100% of the remaining solutions) and one main interacting site on TpII-c_3 around heme I (70% of the remaining solutions).

possibilities indicate two sites on TpI-c_3 (heme III and IV), as selected by the NMR experiments, but also allow the selection of solutions mainly around the heme I of TpII-c_3 (70% of the resulting possibilities) (Figure 10).

Discussion

In sulfate-reducing bacteria of the genus *Desulfovibrio*, sulfate reduction and hydrogen oxidation are spatially separated in the cytoplasm and periplasm, respectively. In the past decade, the electron transport between periplasmic hydrogen oxidation and cytoplasmic sulfate reduction was shown to be mediated through transmembrane redox complexes involving a multiheme cytochrome *c* containing either 16 or nine hemes, namely cytochrome Hmc or 9HcA, respectively, coupled to hydrogenase *via* the tetraheme type I cytochrome c_3.[29,36,37,40,41] A tetraheme cytochrome c_3 associated to an additional transmembrane redox complex was recently described in *D. africanus*[32] and *D. vulgaris*.[34] These new cytochromes form a separate family of tetraheme cytochromes referred to as type II cytochrome c_3.[34] All the similarities between HmcA, 9HcA and TpII-c_3 and their associated redox complexes, support a similar physiological function.[28]

HmcA appears to be involved specifically in the case where hydrogen is used as the sole energy source. Deletion of the hmc operon in *Dv*H impairs growth on hydrogen and sulfate; however, it does not prevent growth on hydrogen indicating that there are other proteins that can fulfill the same role.[44] A likely candidate could be the TpII-c_3 complex as the Hmc and TpII-c_3 complexes are both present in *Dv*H.[29,57] It results from our investigations that neither HmcA nor 9HcA were isolated from *Da* soluble or membrane-bound protein extracts (our unpublished data). Furthermore, these cytochromes were not detected in extracts from *Da* grown on hydrogen sulfate or lactate sulfate media using heme staining in gels.[58] These results suggest that TpII-c_3 is an important electron transfer link in the *Da* hydrogen-sulfate reduction pathway. Moreover, the TpII-c$_3$s from *Da* and *Dv*H, which are periplasmic proteins, differ by their affinity for the membrane. *Dv*H TpII-c_3 is found exclusively in the membrane fraction,[34] whereas the *Da* homologous cytochrome is mainly distributed in the soluble fraction (this work) and loosely bound to the membrane probably due to its highly acidic properties.

Comparative kinetic experiments of *D. africanus* TpI-c_3 and TpII-c_3 reduction by hydrogenase corroborate previous data suggesting that the function of TpII-c_3 is not to receive electrons directly from the periplasmic [NiFeSe] hydrogenase.[31,32] Indeed, the kinetic data clearly indicate that TpI-c_3 is at least 50 times more efficient than TpII-c_3 in the hydrogen consumption reaction catalyzed by hydrogenase. Therefore, TpI-c_3 appears to be the physiological partner of hydrogenase and the results are in agreement with its role as electron shuttle between hydrogenase and TpII-c_3.[31,32] Similarly, *Dv*H TpII-c_3 is less efficient than the TpI-c_3 as an electron acceptor for all three *Dv*H hydrogenases and the reduction of TpII-c_3 is increased in the presence of catalytic amounts of TpI-c_3.[34]

This work reports the first characterization of the interprotein complex between *D. africanus* type I and type II cytochrome c_3 and the structural analysis of the *D. vulgaris* homologous complex improving our understanding of the structural basis of the intracomplex electron transfer between these two tetraheme cytochromes.

Various experimental techniques including gel filtration, analytical ultracentrifugation, cross-linking, microcalorimetry and NMR titration provide evidence that *Da* TpI-c_3 and TpII-c_3 form a complex at low ionic strength. The experiments cited support the role of TpII-c$_3$ as the physiological electron acceptor of TpI-c_3 by demonstrating specific and direct protein/protein interaction. It appears likely that electrostatic forces play an important role in stabilizing the complex between the two proteins as complex formation cannot be detected at high ionic strength. The association constant value determined by microcalorimetric titration was found to be $2.2(\pm 0.5)\times 10^6\ M^{-1}$ at pH 5.5 and the results show that the ionization states of the proteins play a crucial role in the TpI-c_3/TpII-c_3 complex formation. The weak enthalpy changes, ΔH°_{int}, and the large positive entropy values, ΔS°_{int}, indicate an entropy-driven effect. However, the strong ionic strength effect reveals a prominent electrostatic contribution to the interaction. Therefore, it is possible that the large positive entropy changes arise from exclusion of water molecules at the interface. Our thermodynamic results reveal that proton release in combination with water molecules exclusion dominates to produce a net enhancement in enthalpy and entropy.

Electron transfer between proteins generally requires formation of a transient complex that brings together the two redox centers exchanging electrons to achieve a high turnover rate.[59] Electrostatic interactions associated to surface charge complementarity of redox partners play a key role in protein recognition and orientation during electron transfer reactions. The TpI-c_3/TpII-c_3 interaction can be considered as a confirmation of this rule. In order to progress in the structural analysis of the TpI-c_3/TpII-c_3 complex, we have used a strategy combining a soft docking calculation with NMR experimental data. This has been carried out with the *D. vulgaris* cytochrome c$_3$ proteins as this approach was successfully applied to the study of the [Fe] hydrogenase/TpI-c_3 complex from the same microorganism.[54] These data associated to soft docking calculation evidence that the main interaction site involves the surface area around heme IV of TpI-c_3 and heme I region of TpII-c_3 as reported recently in a purely theoretical study.[60] Furthermore, docking studies of the *Da* homologous complex indicate that the highest

number of solutions also implicate heme IV from TpI-c_3 and heme I from TpII-c_3, respectively. In the same way, the involvement of heme I region from *Da* TpII-c_3 was substantiated by NMR titration experiments.

Here, we discuss the properties of the interface of the structural models of the TpI-c_3/TpII-c_3 complex of *Dv*H obtained *via* NMR restrained docking taking into account that the properties of the interface of the *Da* complex are similar. The buried area upon complex formation is close to 1900 A^2 in keeping with the properties of other protein/protein complexes.[61] The composition of the interacting site is in the typical range for electron transfer complexes[62] with about 40% polar and 60% apolar atoms at the interface. Electrostatic interactions dominate the complex interface, in agreement with the strong dependence of the complex formation on ionic strength as shown by microcalorimetric and cross-linking experiments achieved with *Da* complex. In the *Dv*H complex, several lysine residues of the loops surrounding heme IV of TpI-c_3 (K15, K57, K58, K60, K72, K94, K95, K101, and K102) are found at the interface of the complex, mostly interacting with acidic residues (Asp3, Glu8, Asp23, Asp25, Glu29, Glu34, Glu51 and Glu55) of TpII-c_3. The presence of these charged residues located at the interacting site confirms that the electrostatic interactions are the driving force in the formation of complexes involving cytochrome c_3. A rather short distance (close to 4 Å) is observed between the sulfur atoms of two cysteine residues present at the interface including C100 covalently linking heme IV of TpI-c_3 and C36 linking heme I of TpII-c_3. The close approach of cysteine residues leads to a favorable electron-transfer pathway across the intermolecular surfaces.[27,54,56,63] Moreover, structural models pinpoint a tyrosine residue (Y66) of TpI-c_3 at the center of the interface between the two interacting hemes. This aromatic residue could also facilitate electron transfer between the two redox partners.

When one compares the NMR data of the TpI-c_3/TpII-c_3 and TpI-c_3/hydrogenase[54] complexes, three affected residues in the NMR spectra are in common (D59, H70 and D96). In the second place, two other affected residues (M69 and L97) in TpI-c_3/TpII-c_3 complex are closely related to residues (M70 and T99) that undergo chemical shift variations upon TpI-c_3/hydrogenase complex formation. This indicates that the interacting surface involves heme IV in both cases. Moreover, this implies that the same area of the TpI-c_3 is also implicated in the interaction with HmcA.[27] These results exclude the presence of a ternary complex and sustain the model where cytochrome c_3 is an electron shuttle between the periplasmic hydrogenase and membrane-bound TpII-c_3 or HmcA. It is also to be noted that for the case of 9HcA, modeling studies indicated a specific interaction between the negative heme I N-terminal region and the positive heme IV region of TpI-c_3.[29] Furthermore, heme IV from TpI-c_3 exhibits generally the highest redox potential in these tetraheme cytochromes.[64,65] Therefore, electron transfer from hydrogen ($E^{\circ\prime} = -414$ mV) to cytochrome c_3 through the [4Fe-4S] clusters of hydrogenase[66] should be highly favorable from a thermodynamic point of view.

In addition to the main interacting site involving heme IV from TpI-c_3 and heme I from TpII-c_3, in our hands a minor interacting site, which is different in the two complexes, was observed. The characterization at the molecular level of the *Dv*H complex evidences that the minor site implicates heme III of TpI-c_3 and heme I of TpII-c_3 (TpI-c_3/TpII-c_3 molar stoichiometry 1:2). On the contrary, in the *Da* complex the minor site involves heme IV of TpI-c_3 and heme II of TpII-c_3 (molar stoichiometry 2:1). In particular, NMR titration experiments with *Da* complex clearly substantiated that the interacting site associated with heme II of TpII-c_3 is a site of lower affinity (Figure 6). This result appears to be in agreement with the data of cross-linking experiments showing a major band corresponding to a TpI-c_3/TpII-c_3 complex and a minor cross-linked product corresponding to a ternary complex. It is also to be emphasized that in the case of *Dv*H, the minor interaction leads to an unfavorable electron-transfer pathway across the intermolecular surfaces owing to the relative orientation of the heme III/heme I interface. As we found in other complexes, the exposed heme edge of heme I exhibits the methyl groups at the interface while for heme III the propionate groups are present at the interface which is not commonly found. Therefore, the surface-exposed sides of the interacting hemes lack the characteristic S–S contact between cysteine residues covalently linked to these heme groups which represents a possible short electron pathway to facilitate the intermolecular electron transfer.[27,54,56,63] The minor site of *Da* complex exhibits similar properties.

On the basis of these observations, the minor sites of both complexes should be considered as non-physiological sites. In fact, in the case of the TpI-c_3/TpII-c_3 interaction, it is likely that the broad negatively charged surface of *Da* TpII-c_3[33] or the widespread positively charged area of *Dv*H TpI-c_3[34] can bind more than one cytochrome c_3 redox partner giving rise to a ternary complex. Such ternary complex formation between small acidic and basic electron-transfer proteins which may not be of physiological significance has been described.[67,68] In the case of the interaction involving flavodoxin and two cytochrome c_3 molecules, the proposed models for the ternary complex show that only one of the cytochrome molecules can bring a heme group into close contact to the FMN redox group leading to productive electron transfer.[67] However, in the TpI-c_3/TpII-c_3 complexes, taking into account the short distance between the two low affinity interacting hemes, we cannot exclude the hypothesis that the minor sites are physiologically relevant, allowing additional electron entrance or exit gate in these multiheme cytochromes.

Materials and Methods

Proteins

D. africanus TpI-c_3 and TpII-c_3 formerly referred as "basic" and "acidic" cytochrome c_3, respectively, were purified using the procedure reported[31]. The cytochrome concentrations were determined spectrophotometrically using absorption coefficients at 532 nm of 42,900 $M^{-1}\,cm^{-1}$ and 43,120 $M^{-1}\,cm^{-1}$ for oxidized TpI-c_3 and TpII-c_3, respectively, as reported[31]. Purification and activity measurements of [NiFeSe] hydrogenase from *D. africanus* were performed as described.[32,69] TpI-c_3 and ^{15}N-labeled TpI-c_3 from *Dv*H were obtained as reported[55,70]. TpII-c_3 from *Dv*H was purified from the membrane fraction obtained from 270 g of wet cells after solubilization with the zwitterionic detergent 3-(dodecyldimethyl-ammonio)propanesulfonate (SB12) using the procedure reported[34] with the following modifications. After chromatography of the solubilized membrane fraction on DEAE Sepharose Fast Flow column (5 cm × 40 cm; Pharmacia–Amersham), the TpII-c_3 containing fraction was dialyzed and loaded onto a Q Sepharose Fast Flow column (2.6 cm × 17 cm; Pharmacia–Amersham) equilibrated with 20 mM Tris–HCl buffer (pH 7.6) containing 0.2%(w/v) SB12. The column was developed using a stepwise gradient of 0–180 mM NaCl containing 20 mM Tris–HCl and 0.2% SB12 and the cytochrome-containing fraction eluted from the column with 120 mM NaCl. The fraction was then concentrated by ultrafiltration and loaded onto a Sephacryl S100 HR column (2.6 cm × 80 cm; Pharmacia–Amersham) equilibrated with 50 mM Tris–HCl/50 mM NaCl buffer without detergent. The cytochrome-containing fraction from this column was dialyzed against 20 mM Tris–HCl and loaded onto a Q Sepharose HP column (0.8 cm × 5 cm; Pharmacia–Amersham). The column was developed with a stepwise gradient of 0–90 mM NaCl in 20 mM Tris–HCl buffer and TpII-c_3 was eluted with 180 mM NaCl. At this stage, *Dv*H TpII-c_3 exhibited a purity index $A_{528ox}/A_{280ox} = 2.22$ and the yield was 4 mg.

Electrochemistry

Cyclic voltammetry (CV) was carried out using an EG&G 273A potentiostat controlled by EG&G PAR M 270/250 software. A conventional three-electrode system was used consisting of a Metrohm Ag/AgCl/saturated NaCl reference electrode, a platinum auxiliary electrode and a pyrolytic graphite (4 mm diameter rod) working electrode. The electrode was polished with 0.05 μm of alumina slurry. Potentials *versus* the normal hydrogen electrode have been obtained by adding 210 mV to the measured potentials. Prior to each experiment, the solutions were deoxygenated by bubbling high-purity nitrogen. All experiments were carried out at room temperature (23 °C) either under nitrogen or hydrogen atmosphere, in 50 mM Tris–HCl buffer (pH 8.5), unless otherwise specified.

The enzymatic reactions involving *D. africanus* [NiFeSe] hydrogenase and redox partners TpI-c_3, TpII-c_3, as well as the synergic action of TpI-c_3 on TpII-c_3, were studied using the electrochemical technique. In this approach, the electrode is the last electron acceptor in the electron transfer chain ruling out hydrogen oxidation. Under hydrogen atmosphere, the cytochrome enzymatically reduced by hydrogenase is electrochemically re-oxidized at the electrode, and an enhanced anodic current is detected. Kinetic data for the catalytic oxidation of hydrogen in the presence of hydrogenase and cytochromes were obtained using the theoretical model proposed by Nicholson & Shain.[71] Briefly, the dependence of the ratio of the kinetically controlled to diffusion-controlled current on the scan rate, v, allowed the determination of the kinetic parameter, $\lambda = k'(RT/nF) \times 1/v$ (where k' is the pseudo-first-order rate constant of the homogeneous chemical reaction between the enzyme and the cytochrome). The second-order rate constant k was finally obtained by plotting k' against the hydrogenase concentration.

Cross-linking reaction

1-Cyclohexyl-3-(2-morpholinoethyl) carbodiimide-methyl-*p*-toluenesulfonate (CME-CDI) is a water-soluble carbodiimide which catalyzes the formation of amide bonds between side-chain carboxylic and amino groups of proteins involved in ion pairing.[72] Covalent cross-linking was carried out by treatment of *D. africanus* TpI-c_3 (75 μM) and TpII-c_3 (76 μM) in 25 mM Mes buffer (pH 6.0) with 15 mM CME-CDI in a final volume of 35 μl for 60 min at 25 °C. The reaction was stopped by adding ammonium acetate to 0.1 M final concentration.

Analytical procedures

Gel filtration chromatography

Gel filtration chromatography of the *Da* TpI-c_3/TpII-c_3 complex was performed on a Sephadex G-75 column (1.5 cm × 85 cm) equilibrated with 10 mM sodium cacodylate buffer (pH 5.6).[73] Chromatography on Sephadex G-75 was also carried out in buffer supplemented with 50 mM NaCl to raise the ionic strength. The following molecular mass standards were used: cytochrome *c*, 12.4 kDa; myoglobin, 18.8 kDa; chymotrypsinogen, 25.5 kDa; ovalbumin, 45 kDa and bovine serum albumin, 68 kDa. The protein content of the fractions eluted from the column was determined spectrophotometrically at 280 nm and 410 nm for the molecular mass standards and the cytochromes c_3, respectively.

Gel electrophoresis

SDS/gel electrophoresis was performed as described,[74] with 11.5%(w/v) polyacrylamide running gel. Protein samples for SDS/gel electrophoresis were previously heated at 100 °C for 5 min in the presence of 2% (w/v) SDS and 1 mM mercaptoethanol. Protein bands were visualized by staining with Coomassie blue R250.

Amino acid analysis

The amino acid composition of cross-linked products was determined by the ninhydrin method after hydrolysis for 24 h with 6 M HCl by means of a Beckman model System 6300 amino acid analyser.

Analytical ultracentrifugation

Samples of *Da* TpI-c_3 and TpII-c_3 were equilibrated in 10 mM cacodylate buffer (pH 5.6) by ultrafiltration using Centricon-10 concentrators (10,000 M_W cut-off, Amicon). Sedimentation equilibrium experiments were performed with a Beckman Optima XL-A analytical ultracentrifuge equipped with absorbance optics, using an AN55Ti rotor.

A short column experiment was performed using 60 μl of TpI-c_3 (from 0.1 mg/ml to 0.7 mg/ml), TpII-c_3 (from 0.5 mg/ml to 2.8 mg/ml) or various concentrations of TpI-c_3 (from 0.01 mg/ml to 2.8 mg/ml) mixed with 0.25 mg/ml of TpII-c_3 in the six-channel centerpieces of charcoal-filled Epon. Measurements were carried out at three successive speeds (18,000, 20,000 and 32,000 rpm) by taking scans at the appropriate wavelength (530, 570, 580 and 600 nm) when sedimentation equilibrium was reached. The equilibrium temperature was 20 °C. High-speed sedimentation (50,000 rpm) was conducted afterwards for baseline correction. The weight-average molecular masses (M_w) were determined by fitting a sedimentation equilibrium model for a single sedimenting solute to individual datasets with EQASSOC programs, supplied by Beckman.[75] The partial specific volumes of TpI-c_3 and TpII-c_3 were assumed to be 0.72 ml/g at 20 °C. The solvent density and the viscosity were assumed to be 1 and 0.002 poise, respectively.

Microcalorimetry

Reagents

TpI-c_3 and TpII-c_3 solutions were prepared in the appropriate buffer to obtain concentration values close to 10 μM and 200 μM for *D. africanus* or 3 mM and 0.2 mM for *D. vulgaris*. In order to obtain TpI-c_3 and TpII-c_3 under identical buffering conditions, the protein solutions were dialyzed extensively and concentrated by ultrafiltration using Centricon-10 concentrators (10,000 M_W cut-off; Amicon).

Isothermal titration calorimetry (ITC)

Equilibrium binding experiments designed to study the interaction between TpI-c_3 and TpII-c_3 were performed at 310 K using a 2277 Thermal Activity Monitor calorimeter (Thermometric, Sweden) equipped with a titration unit. Data acquisition and analyses were carried out using DIGITAM 4.1 software (Thermometric, Sweden).

For the *Da* cytochromes, titration was performed as follows. Aliquots (3 μl) of TpII-c_3 solution were injected, at 300 s time intervals, from a 250 μl syringe into the calorimeter cell containing TpI-c_3 solution (0.9 ml) to achieve a complete binding isotherm. The effective heat of binding was obtained by subtracting the heat of dilution (measured by additional injections of TpII-c_3 solution after saturation) from the heat of reaction. Binding enthalpy (ΔH°), the affinity constant (K_a) and stoichiometry (n) were then obtained by fitting the experimental corrected binding isotherm to a model, incorporated into the DIGITAM software, assuming one set of binding sites. Changes in free energy (ΔG°) and entropy (ΔS°) were obtained by the calculation:

$$\Delta G^\circ = -RT \ln K_a = \Delta H^\circ - T\Delta S^\circ$$

According to the methodology described, ITC was used in a first set of experiments to investigate the effect of ionic strength on the interaction. Titrations were thus carried out in 10 mM cacodylate buffer (pH 5.5) with 0, 50 and 100 mM NaCl, respectively. In a separate second set, the effect of pH on TpI-c_3/TpII-c_3 binding was studied at pH 5.5 with cacodylate or Mes buffers, and at pH 6.0, pH 6.5 and pH 7.0 with phosphate or Mes buffers. In all experiments the ionic strength was maintained constant by adjustment of buffer concentrations.

For the *Dv*H cytochromes, titration was carried out under identical experimental conditions except that the TpI-c_3 solution was injected into the calorimeter cell containing the TpII-c_3 solution.

NMR experiments

All the NMR experiments were recorded on a Bruker Avance DRX 500 spectrometer to perform the titration of *Da* TpI-c_3/TpII-c_3 complex formation. 1D-NMR experiments were carried out at 303 K and pH 6.07. During titration, small amounts of 850 μM TpI-c_3 were added to the 85 μM TpII-c_3 sample. The spectral width was 70 ppm for the 32 K data points and 160 scans accumulated. NMR spectra were obtained using presaturation of water and processed using xwinnmr provided by Bruker. The chemical shifts were referenced to the H_2O resonance (4.76 ppm at 303 K).

2D NMR experiments (^{15}N-^1H HSQC) were recorded on a 1:1 *Dv*H TpI-c_3/TpII-c_3 complex, at 57 μM concentration, in potassium phosphate buffer (pH 5.9) at 308 K. The spectra were acquired accumulating 224 scans per free induction decay, with 256 complex points in F_1 and 2000 complex points in F_2. The spectral widths were 6000 Hz for ^{15}N and 2000 Hz for ^1H. ^1H chemical shift variations were referenced with H_2O resonance and ^{15}N chemical shifts were referenced indirectly using the $^1H/^{15}N$ frequency ratio 0.1013291118.[76] ^1H and ^{15}N chemical shift assignments of *Dv*H TpI-c_3 have been reported (accession number BMRB-5239). In HSQC experiments, the chemical shift variations were observed on exposed NH groups located at the interacting site, the side-chains of the corresponding residues being buried in the molecule (this is the case for hydrophobic residues such as Val or Ile). Residues involved in protein/protein interactions (like basic residues) have exposed side-chains and buried NH groups. The NH resonances of these residues may be not affected by formation of the complex. Thus, chemical shift variations give the mapping of an interacting site.

Crystallization

Crystals of *Da* TpI-c_3 were grown by the vapor diffusion method in hanging drops. The 0.5 ml well solution contained 3.2 M NaH_2PO_4/K_2HPO_4 and the 4 μl drops contained 2 μl of protein at a concentration of 8 mg ml^{-1} and 2 μl of well solution. Crystals grew within a few days and belonged to the space group $C2$ with cell parameters $a = 100.9$ Å, $b = 46.3$ Å, $c = 54.8$ Å and $\beta = 119°$. They contain two monomers per asymmetric unit, which corresponds to a Matthews volume, V_M, of 2.3 $Å^3$ Da^{-1}.

Data collection, phasing and refinement

The crystals were transferred to a cryoprotectant solution that consisted of 4.1 M $NH_4(SO_4)_2$. Subsequently the crystals, mounted in cryo-loops, were flash frozen in a cold nitrogen stream at 100 K. The X-ray data sets from native protein crystals were collected at the European Synchrotron Radiation Facility (Grenoble, France) on beamlines ID14-EH2 at $\lambda = 0.93$ Å and ID29 at the wavelength of the maximum of the iron absorption edge ($\lambda = 1.73891$ Å), measured on the *Da* TpI-c_3 crystal. The data were processed and integrated with DENZO[77] and scaled using SCALA of the CCP4[78] suite. The data collection and phasing statistics are given in Table 2.

Table 2. Summary of crystallographic statistics

Data sets	Native	λ_1
Wavelength (Å)	0.93	1.73891
Resolution range (Å)	48.0–1.50	27.0–2.00
Completeness (%)	94.8 (71.8)[a]	95.9(92.6)
Redundancy	7.6 (7.5)	4.2 (4.3)
$I/\sigma(I)$	20.2 (11.3)	23.6 (15.2)
R_{sym}[b]	0.059 (0.061)	0.056 (0.081)
A. Phasing statistics		
Dispersive/anomalous difference (%)	–/3.6	15.3/7.9
Figure of merit (overall)	0.739 (0.788)[c]	
B. Refinement statistics		
Resolution range (Å)	48 – 1.50	
Number of unique reflections	22,893	
R_{cryst} (%)[d]	18.8	
R_{free} (%)[e]	22.7	
r.m.s. deviation bond lengths	0.009	
r.m.s. deviation bond angles (°)	1.9	
Residues in most favored region of the Ramachandran plot (%)	82	
Residues in additionally allowed regions of the Ramachandran plot (%)	18	

[a] Numbers in parantheses indicate values for the highest resolution bin.
[b] $R_{sym}=\Sigma[I_i-\langle I\rangle]/\Sigma[\langle I\rangle]$ where i is the ith measurement and $\langle I\rangle$ is the weighted mean of I.
[c] Figure of merit value in parentheses is calculated after density modification with DM.
[d] $R_{cryst}=\Sigma||F_{obs}|-|F_{calc}||/\Sigma|F_{obs}|$.
[e] R_{free} is the same as R_{cryst} for 5% of the data omitted from refinement totaling 1407 reflections.

The crystal structure of *Da* TpI-c_3 cytochrome was solved by the SAD method using the programs SOLVE[79] and SHARP.[80] In a first step seven of the eight iron positions were found by SOLVE. These sites were subsequently submitted to refinement and phase calculation with SHARP and the eighth iron site was easily identified in the residual electron density map. In a second step, phases were again calculated with SHARP using all eight heavy-atom positions and subsequently submitted to density modification with DM.[78] The model for the two copies of cytochrome c_3 within the asymmetric unit was then built into the experimental electron density map using the program suite ARP/wARP.[81]

The refinement of the atomic structure of *Da* TpI-c_3 was performed with REFMAC5[78] and small adjustments of the structural model were done with TURBO-FRODO.[82] The final refinement statistics are given in Table 2.

Protein docking

A three-dimensional model of *Dv*H TpII-c_3 was generated by substituting the residues of the *Dv*H cytochrome in *Da* TpII-c_3 structure (PDB id code 3cao) by homology modelling using Modeller 6.0. For *Da* TpI-c_3/TpII-c_3 complex modelling, the protein coordinates of *Da* TpI-c_3 (PDB id code 2bq4) and *Da TpII-c_3* (PDB id code 3cao) were used, and for the *Dv*H TpI-c_3/TpII-c_3 complex, the protein coordinates of *Dv*H TpI-c_3 (PDB id code 2cth) and the model of *Dv*H TpII-c_3 were employed.

Molecular interaction simulations were executed using the docking program BiGGER.[83] This algorithm performs a complete and systematic search in the binding space of both molecules. A population of 1000 candidates of cytochrome TpI/TpII docked geometries was generated and selected, based on the geometric complementarity and amino acid pairwise affinities between the two molecular surfaces. In this process, the algorithm enables implicit treatment of molecular flexibility. A distance of 20 Å maximum between hemes of TpI-c_3 and TpII-c_3 for the *D. africanus* docking was used to filter the 1000 *ab initio* solutions in order to eliminate false positives. The resulting putative docked solutions were then clustered and ranked according to an interaction scoring function developed in BiGGER.

Protein Data Bank accession codes

The coordinates as well as the experimental structure factors have been deposited with the RCSB Protein Data Bank and are assigned idcodes 2bq4 and r2bq4sf, respectively.

Acknowledgements

We are indebted to Nicole Forget for skillful technical assistance in the purification of proteins and to Marielle Bauzan for growing large-scale cultures of *D. africanus* and *D. vulgaris*.

References

1. Postgate, J. R. (1979). *The Sulphate-Reducing Bacteria*, Cambridge University Press, Cambridge p. 151.
2. LeGall, J. & Fauque, G. (1988). Dissimilatory reduction of sulfur compounds. In *Bioenergetic strategies of the sulfate-reducing bacteria* (Zenhder, A. J. B., ed.), pp. 587–639, Wiley, New York.
3. Peck, H. D., Jr (1993). Bioenergetic strategies of the sulfate-reducing bacteria. In *Vectorial electron transport in Desulfovibrio vulgaris* (Marburg) growing on hydrogen plus sulfate as sole energy source (Odom, J. M. & Singleton, R., eds), pp. 41–76, Springer, Berlin.

4. Badziong, W. & Thauer, R. K. (1980). Vectorial electron transport in *Desulfovibrio vulgaris* (Marburg) growing on hydrogen plus sulfate as sole energy source. *Arch. Microbiol.* **125**, 167–174.
5. Brandis, A. & Thauer, R. K. (1981). Growth of *Desulfovibrio* species on hydrogen and sulfate as sole energy source. *J. Gen. Microbiol.* **126**, 249–252.
6. Postgate, J. R. (1952). Growth of sulfate-reducing bacteria in sulfate-free media. *Research (London)*, **5**, 189–190.
7. Vosjan, J. H. (1975). Respiration and fermentation of the sulfate-reducing bacterium *Desulfovibrio desulfuricans* in continuous culture. *Plant Soil*, **43**, 141–152.
8. Bryant, M. P., Campbell, L. L., Reddy, C. A. & Crabil, M. R. (1977). Growth of *Desulfovibrio* in lactate or ethanol media low in sulfate in association with H_2-utilizing methanogenic bacteria. *Appl. Environ. Microbiol.* **33**, 1162–1169.
9. Fauque, G., Peck, H. D., Jr, Moura, J. J. G., Huynh, B. H., Berlier, Y., DerVartanian, D. V. *et al*. (1988). The three classes of hydrogenases from sulfate-reducing bacteria of the genus *Desulfovibrio*. *FEMS Microbiol. Rev.* **54**, 299–344.
10. Hatchikian, E. C., Fernandez, V. M. & Cammack, R. (1990). The hydrogenase of sulfate-reducing bacteria: physiological, biochemical and catalytic aspects. Microbiology and biochemistry of strict anaerobes involved in intersecies H_2 transfer. In *Structural and functional approach toward a classification of the complex cytochrome c* system found in sulfate-reducing bacteria (Bélaich, J. P., Bruschi, M. & Garcia, J. L., eds), pp. 53–73, Plenum Press, New York.
11. Moura, J. J. G., Costa, C., Liu, M.-Y., Moura, I. & LeGall, J. (1991). Structural and functional approach toward a classification of the complex cytochrome *c* system found in sulfate-reducing bacteria. *Biochim. Biophys. Acta*, **1058**, 61–66.
12. Pereira, I. A. C., Teixeira, M. & Xavier, A. V. (1998). Hemeproteins in anaerobes. *Struct. Bonding (Berlin)*, **91**, 65–89.
13. Coutinho, I. B. & Xavier, A. V. (1994). Tetraheme cytochromes. *Methods Enzymol.* **243**, 119–140.
14. Yagi, T., Honya, M. & Tamiya, N. (1968). Purification and properties of hydrogenases of different origins. *Biochim. Biophys. Acta*, **153**, 699–705.
15. Bell, G. R., Lee, J.-P., Peck, H. D., Jr & LeGall, J. (1978). Reactivity of *Desulfovibrio gigas* hydrogenase toward artificial and natural electron donors or acceptors. *Biochimie*, **60**, 315–320.
16. Nivière, V., Hatchikian, E. C., Bianco, P. & Haladjian, J. (1988). Kinetic studies of electron transfer between hydrogenase and cytochrome c_3 from *Desulfovibrio gigas*. Electrochemical properties of cytochrome c_3. *Biochim. Biophys. Acta*, **935**, 34–40.
17. Haser, R., Pierrot, M., Frey, M., Payan, J. P., Astier, M., Bruschi, J. & LeGall, J. (1979). Structure and sequence of the multihaem cytochrome c_3. *Nature*, **282**, 806–810.
18. Higuchi, Y., Bando, S., Kusunoki, M., Matsuura, Y. & Yasuoka, N. (1981). The structure of cytochrome c_3 from *Desulfovibrio vulgaris* Miyazaki at 2.5 Å resolution. *J. Biochem.* **89**, 1659–1662.
19. Morimoto, Y., Tani, T., Okumura, H., Higuchi, Y. & Yasuoka, N. (1991). Effects of amino acid substitution on three-dimensional structure: an X-ray analysis of cytochrome c_3 from *Desulfovibrio vulgaris* Hildenborough at 2 Å resolution. *J. Biochem.* **110**, 532–540.
20. Czjzek, M., Payan, F., Guerlesquin, F., Bruschi, M. & Haser, R. (1994). Crystal structure of cytochrome c_3 from *Desulfovibrio desulfuricans* Norway at 1.7 Å resolution. *J. Mol. Biol.* **243**, 653–667.
21. Morais, J., Palma, P. N., Frazao, C., Caldeira, J., LeGall, J., Moura, I. *et al*. (1995). Structure of the tetraheme cytochrome from *Desulfovibrio desulfuricans* ATCC 27774: X-ray diffraction and electron paramagnetic resonance studies. *Biochemistry*, **34**, 12830–12841.
22. Matias, P. M., Morais, J., Coelho, R., Carrondo, M. A., Wilson, K., Dauter, Z. & Sieker, L. (1996). Cytochrome c_3 from *Desulfovibrio gigas*: crystal structure at 1.8 Å resolution and evidence for a specific calcium-binding site. *Protein Sci.* **5**, 1342–1354.
23. Messias, A. C., Kastrau, D. H., Costa, H. S., LeGall, J., Turner, D. L., Santos, H. & Xavier, A. V. (1998). Solution structure of *Desulfovibrio vulgaris* (Hildenborough) ferrocytochrome c_3: structural basis for functional cooperativity. *J. Mol. Biol.* **281**, 719–739.
24. Harada, E., Fukuoka, Y., Ohmura, T., Fukunishi, A., Kawai, G., Fujiwara, T. & Akutsu, H. (2002). Redox-coupled conformational alternations in cytochrome c_3 from *D. vulgaris* Miyazaki F on the basis of its reduced solution structure. *J. Mol. Biol.* **319**, 767–778.
25. Czjzek, M., Guerlesquin, F., Bruschi, M. & Haser, R. (1996). Crystal structure of a dimeric octaheme cytochrome c_3 (M_r 26,000) from *Desulfovibrio desulfuricans* Norway. *Structure*, **4**, 395–404.
26. Frazao, C., Sieker, L., Sheldrick, G., Lamzin, V., LeGall, J. & Carrondo, M. A. (1999). Ab initio structure solution of a dimeric cytochrome c_3 from *Desulfovibrio gigas* containing disulfide bridges. *J. Biol. Inorg. Chem.* **4**, 162–165.
27. Czjzek, M., ElAntak, L., Zamboni, V., Morelli, X., Dolla, A., Guerlesquin, F. & Bruschi, M. (2002). The crystal structure of the hexadeca-heme cytochrome Hmc and a structural model of its complex with cytochrome c_3. *Structure*, **10**, 1677–1686.
28. Matias, P. M., Coelho, A. V., Valente, F. M. A., Placido, D., LeGall, J., Xavier, A. V. *et al*. (2002). Sulfate respiration in *Desulfovibrio vulgaris* Hildenborough: structure of the 16-heme cytochrome c HmcA at 2.5 Å resolution and a view of its role in transmembrane electron transfer. *J. Biol. Chem.* **277**, 47907–47916.
29. Matias, P. M., Saraiva, L. M., Soares, C. M., Coelho, A. V., LeGall, J. & Carrondo, M. A. (1999). Nine-haem cytochrome c from *Desulfovibrio desulfuricans* ATCC 27774: primary sequence determination, crystallographic refinement at 1.8 Å and modelling studies of its interaction with the tetrahaem cytochrome c_3. *J. Biol. Inorg. Chem.* **4**, 478–494.
30. Umhau, S., Fritz, G., Diederichs, K., Breed, J., Welte, W. & Kroneck, P. M. (2001). Three-dimensional structure of the nonaheme cytochrome c from *Desulfovibrio desulfuricans* Essex in the Fe(III) state at 1.89 Å resolution. *Biochemistry*, **40**, 1308–1316.
31. Pieulle, L., Haladjian, J., Bonicel, J. & Hatchikian, E. C. (1996). Biochemical studies of the c-type cytochromes of the sulfate reducer *Desulfovibrio africanus*. Characterization of two tetraheme cytochromes c_3 with different specificity. *Biochim. Biophys. Acta*, **1273**, 51–61.
32. Magro, V., Pieulle, L., Forget, N., Guigliarelli, B., Petillot, Y. & Hatchikian, E. C. (1997). Further characterization of the two tetraheme cytochromes c_3 from *Desulfovibrio africanus*: nucleotide sequence, EPR spectroscopy and biological activity. *Biochim. Biophys. Acta*, **1342**, 149–163.
33. Norager, S., Legrand, P., Pieulle, L., Hatchikian, E. C. & Roth, M. (1999). Crystal structure of the oxidized

and reduced acidic cytochrome c_3 from *Desulfovibrio africanus*. *J. Mol. Biol.* **290**, 881–902.
34. Valente, F. M. A., Saraiva, L. M., LeGall, J., Xavier, A. V., Teixeira, M. & Pereira, I. A. C. (2001). A membrane-bound cytochrome c_3: a Type II cytochrome c_3 from *Desulfovibrio vulgaris* Hildenborough. *Chem.Biol.Chem.* **2**, 895–905.
35. Pereira, P. M., Pacheco, I., Turner, D. L. & Louro, R. O. (2002). Structure–function relationship in type II cytochrome c_3 from *Desulfovibrio africanus*: a novel function in a familiar heme core. *J. Biol. Inorg. Chem.* **7**, 815–822.
36. Rossi, M., Pollock, W. B. R., Reij, M. W., Keon, R. G., Fu, R. & Voordouw, G. (1993). The hmc operon of *Desulfovibrio vulgaris* Hildenborough encodes a potential transmembrane redox protein complex. *J. Bacteriol.* **175**, 4699–4711.
37. Saraiva, L. M., da Costa, P. N., Conte, C., Xavier, A. V. & LeGall, J. (2001). In the facultative sulphate/nitrate reducer *Desulfovibrio desulfuricans* ATCC 27774, the nine-haem cytochrome c is part of a membrane-bound redox complex mainly expressed in sulphate-grown cells. *Biochim. Biophys. Acta*, **1520**, 63–70.
38. Voordouw, G. & Brenner, S. (1986). Cloning and sequencing of the gene encoding cytochrome c_3 from *Desulfovibrio vulgaris* (Hildenborough). *Eur. J. Biochem.* **159**, 347–351.
39. Aubert, C., Leroy, G., Bruschi, M., Wall, J. D. & Dolla, A. (1997). A single mutation in the heme 4 environment of *Desulfovibrio desulfuricans* Norway cytochrome c_3 (M_r 26,000) greatly affects the molecule reactivity. *J. Biol. Chem.* **272**, 15128–15134.
40. Pereira, I. A. C., Romao, C. V., Xavier, A. V., LeGall, J. & Teixeira, M. (1998). Electron transfer between hydrogenases and mono- and multiheme cytochromes in *Desulfovibrio* ssp. *J. Biol. Inorg. Chem.* **3**, 494–498.
41. Aubert, C., Brugna, M., Dolla, A., Bruschi, M. & Giudici-Orticoni, M. T. (2000). A sequential electron transfer from hydrogenases to cytochromes in sulfate-reducing bacteria. *Biochim. Biophys. Acta*, **1476**, 85–92.
42. Fritz, G., Griesshaber, D., Seth, O. & Kroneck, P. M. H. (2001). Nonaheme cytochrome c, a new physiological electron acceptor for [Ni,Fe] hydrogenase in the sulfate-reducing bacterium *Desulfovibrio desulfuricans* Essex: primary sequence, molecular parameters, and redox properties. *Biochemistry,* **40**, 1317–1324.
43. Keon, R. G., Fu, R. & Voordouw, G. (1997). Deletion of two downstream genes alters expression of the hmc operon of *Desulfovibrio vulgaris* subsp. vulgaris Hildenborough. *Arch. Microbiol.* **167**, 376–383.
44. Dolla, A., Pohorelic, B. K., Voordouw, J. K. & Voordouw, G. (2000). Deletion of the hmc operon of *Desulfovibrio vulgaris* subsp. vulgaris Hildenborough hampers hydrogen metabolism and low-redox potential niche establishment. *Arch. Microbiol.* **174**, 143–151.
45. Steger, J. L., Vincent, C., Ballard, J. D. & Krumholz, L. R. (2002). *Desulfovibrio* sp. genes involved in the respiration of sulfate during metabolism of hydrogen and lactate. *Appl. Environ. Microbiol.* **68**, 1932–1937.
46. Nivière, V. (1989). Etudes biochimiques et physico-chimiques de deux hydrogénases à nickel de bactéries sulfato-réductrices du genre Desulfovibrio. p. 147, Thèse de Doctorat d'Université. Université d'Aix-Marseille II.
47. Lojou, E., Pieulle, L., Guerlesquin, F. & Bianco, P. (2002). From the protein-polypeptide model system to the interaction between physiological partners using electrochemistry. *J. Electroanal. Chem.* **523**, 150–159.
48. Andrews, P. (1964). Estimation of the molecular weights of proteins by Sephadex gel-filtration. *Biochem. J.* **91**, 222–233.
49. Baker, B. M. & Murphy, K. P. (1996). Evaluation of linked protonation effects in protein binding reactions using isothermal titration calorimetry. *Biophys. J.* **71**, 2049–2055.
50. Kabsch, W. & Sanders, C. (1983). Dictionary of protein secondary structure: Pattern recognition of hydrogen-bonded and geometrical features. *Biopolymers*, **22**, 2577–2637.
51. Stellwagen, E. (1978). Haem exposure as the determinate of oxidation–reduction potential of haem proteins. *Nature*, **275**, 73–74.
52. Cambillau, C., Frey, M., Mossé, J., Guerlesquin, F. & Bruschi, M. (1988). Model of a complex between the tetrahemic cytochrome c_3 and the ferredoxin I from *Desulfovibrio desulfuricans* (Norway strain). *Proteins: Struct. Funct. Genet.* **4**, 63–70.
53. Matias, P. M., Soares, C. M., Saraiva, L. M., Coelho, R., Morais, J., LeGall, J. & Carrondo, M. A. (2001). [NiFe] hydrogenase from *Desulfovibrio desulfuricans* ATCC 27774: gene sequencing, three-dimensional structure determination and refinement at 1.8 Å and modelling studies of its interaction with the tetrahaem cytochrome *c*3. *J. Biol. Inorg. Chem.* **6**, 63–81.
54. El Antak, L., Morelli, X., Bornet, O., Hatchikian, E. C., Czjzek, M., Dolla, A. & Guerlesquin, F. (2003). The cytochrome c_3-[Fe]-hydrogenase electron-transfer complex: structural model by NMR restrained docking. *FEBS Letters*, **548**, 1–4.
55. El Antak, L., Bornet, O., Morelli, X., Dolla, A. & Guerlesquin, F. (2002). Sequencial NMR assignment of the ferri-cytochrome c_3 from *Desulfovibrio vulgaris* Hildenborough. *J. Biomol. NMR*, **23**, 69–70.
56. Morelli, X., Dolla, A., Czjzek, M., Palma, N., Blasco, F., Krippahl, L. *et al*. (2000). Heteronuclear NMR and soft docking: an experimental approach for a structural model of the cytochrome c_{553}-ferredoxin complex. *Biochemistry,* **39**, 2530–2537.
57. Heidelberg, J. H., Seshadri, R., Haveman, S. A., Hemme, C. L., Paulsen, I. T., Kolonay, J. F. *et al*. (2004). The genome sequence of the anaerobic sulfate-reducing bacterium, *Desulfovibrio vulgaris* Hildenborough. *Nature Biotechnol.* **22**, 554–559.
58. Goodhew, C. F., Brown, K. R. & Pettigrew, G. W. (1986). Heme-staining in gels, useful tool in the study of *c*-type cytochromes. *Biochim. Biophys. Acta*, **852**, 288–294.
59. Bendall, D. S. (1996). Interprotein electron transfer. In *Modeling electron transfer thermodynamics in protein complexes: interaction between two cytochromes c*3 (Bendall, D. S., ed.), pp. 43–68, BIOS Scientific Publishers, Oxford, UK.
60. Teixeira, V. H., Baptista, A. M. & Soares, C. M. (2004). Modeling electron transfer thermodynamics in protein complexes: interaction between two cytochromes *c*3. *Biophys. J.* **86**, 2773–2785.
61. LoConte, L., Chothia, C. & Janin, J. (1999). The atomic structure of protein–protein recognition sites. *J. Mol. Biol.* **285**, 2177–2198.
62. Williams, P. A., Fülöp, V., Leung, Y.-C., Chan, C., Moir, J. W. B., Howlett, G. *et al*. (1995). Pseudospecific docking surfaces on electron transfer proteins as illustrated by pseudoazurin, cytochrome c_{550} and cytochrome cd_1 nitrite reductase. *Nature Struct. Biol.* **2**, 975–982.

63. Pieulle, L., Nouailler, M., Morelli, X., Cavazza, C., Gallice, P., Blanchet, S. *et al*. (2004). Multiple orientations in a physiological complex: the pyruvate-ferredoxin oxidoreductase-ferredoxin system. *Biochemistry*, **43**, 15480–15493.
64. Picarra-Pereira, M. A., Turner, D., LeGall, J. & Xavier, A. V. (1993). Structural studies on *Desulfovibrio gigas* cytochrome c_3 by two-dimensional ^{1}H-nuclear-magnetic-resonance spectroscopy. *Biochem. J.* **294**, 904–915.
65. Turner, D. L., Salguiero, C. A., Catarino, T., LeGall, J. & Xavier, A. V. (1996). NMR studies of cooperativity in the tetraheme cytochrome c_3 from *Desulfovibrio vulgaris*. *Eur. J. Biochem.* **241**, 723–731.
66. Cammack, R., Patil, D. S., Hatchikian, E. C. & Fernandez, V. (1987). Nickel and iron-sulphur centres in *Desulfovibrio gigas* hydrogenase: ESR spectra, redox properties and interactions. *Biochim. Biophys. Acta*, **912**, 98–109.
67. Palma, P. N., Moura, I., LeGall, J., Van Beeumen, J., Wampler, J. E. & Moura, J. J. G. (1994). Evidence for a ternary complex formed between flavodoxin and cytochrome c_3: ^{1}H-NMR and molecular modeling studies. *Biochemistry*, **33**, 6394–6407.
68. Park, J.-S., Kano, K., Morimoto, Y., Higuchi, Y., Yasuoka, N., Ogata, M. *et al*. (1991). ^{1}H NMR studies on ferricytochrome c_3 from *Desulfovibrio vulgaris* Miyazaki F and its interaction with ferredoxin I. *J. Biomol. NMR*, **1**, 271–282.
69. Nivière, V., Forget, N., Gayda, J. P. & Hatchikian, E. C. (1986). Chracterization of the soluble hydrogenase from *Desulfovibrio africanus*. *Biochem. Biophys. Res. Commun.* **139**, 658–665.
70. LeGall, J., Bruschi, M. & DerVartanian, D. V. (1971). Electron paramagnetic resonance and light absorption studies on *c*-type cytochromes of the anaerobic sulfate sulfate reducer *Desulfovibrio*. *Biochim. Biophys. Acta*, **234**, 499–512.
71. Nicholson, R. S. & Shain, I. (1964). Theory of stationary electrode polarography. Single scan and cyclic methods applied to reversible, irreversible, and kinetic systems. *Anal. Chem.* **36**, 706–723.
72. Chaillan, C., Rogalska, E., Chapus, C. & Lombardo, D. (1989). A cross-linked complex between horse pancreatic lipase and colipase. *FEBS Letters*, **257**, 443–446.
73. Whitaker, J. R. (1963). Determination of molecular weights of proteins by gel filtration on Sephadex. *Anal. Chem.* **35**, 1950–1953.
74. Laemmli, U. K. (1970). Cleavage of structural proteins during the assembly of the head of bacteriophage T4. *Nature*, **227**, 680–685.
75. Minton, A.P. (1994). Conservation of signal: a new algorithm for the elimination of the reference concentration as an independently variable parameter in the analysis of sedimentation equilibrium. In *Modern Analytical Ultracentrifugation* (Schuster, T. M. & Laue, T. M., eds), pp. 81–93, Birkhauser, Boston.
76. Wishart, D., Bigam, C., Yao, J., Abildgaard, F., Dyson, J., Oldfield, E. *et al*. (1995). ^{1}H, ^{13}C and ^{15}N chemical shift referencing in biomolecular NMR. *J. Biomol. NMR*, **6**, 135–140.
77. Ottwinowski, Z. (1993). *DENZO: An Oscillation Data Processing Program for Macromolecular Protein*, Yale University, New Haven.
78. Computational Collaboration Program 4. (1994). The CCP4 suite: programs for protein crystallography. *Acta Crystallog. sect. D*, **50**, 760–763.
79. Terwilliger, T. C. & Berendzen, J. (1999). Evaluation of macromolecular electron-density map quality using the correlation of local r.m.s. density. *Acta Crystallog. sect. D*, **55**, 1872–1877.
80. La Fortelle, E. & Bricogne, G. (1997). In *Methods in Enzymology, Macromolecular Cystallography* (Sweet, R. M. & Carter, C. W., Jr, eds), vol. 276, pp. 472–494, Academic Press, New York.
81. Lamzin, V. S., Perrakis, A. & Wilson, K. S. (2001). The ARP/wARP suite for automated construction and refinement of protein models. *Int. Tables for Crystallography. Crystallography of Biological Macromolecules*, vol F, (Rossman, M.G. & Arnold, E., eds), pp. 720–722, Kluwer Academic Publishers, Dordrecht, The Netherlands.
82. Roussel, A. & Cambillau, C. (1991). TURBO-FRODO program. In *Silicon Graphics Geometry Partners Directory 88*. Mountain View, CA, USA.
83. Palma, P. N., Krippahl, L., Wampler, J. E. & Moura, J. J. G. (2000). BiGGER: a new (soft) docking algorithm for predicting protein interactions. *Proteins: Struct. Funct. Genet.* **39**, 372–384.

Edited by M. F. Summers

(Received 30 May 2005; received in revised form 30 August 2005; accepted 13 September 2005)
Available online 29 September 2005